REPORT DOCUMENTATION PAGE		READ INSTRUCTIONS BEFORE COMPLETING FORM
1. REPORT NUMBER AFIT/CI/NR 86-137T	2. GOVT ACCESSION NO.	3. RECIPIENT'S CATALOG NUMBER
4. TITLE (and Subtitle) Mesoscale Convective Complex vs. Non-Mesoscale Convective Complex Thunderstorms: A Comparison of Selected Meteorological Variables		5. TYPE OF REPORT & PERIOD COVERED THESIS/~~DISSERTATION~~
		6. PERFORMING ORG. REPORT NUMBER
7. AUTHOR(s) Michael Eugene Hoofard		8. CONTRACT OR GRANT NUMBER(s)
9. PERFORMING ORGANIZATION NAME AND ADDRESS AFIT STUDENT AT: Texas A&M University		10. PROGRAM ELEMENT, PROJECT, TASK AREA & WORK UNIT NUMBERS
11. CONTROLLING OFFICE NAME AND ADDRESS AFIT/NR WPAFB OH 45433-6583		12. REPORT DATE 1986
		13. NUMBER OF PAGES 80
14. MONITORING AGENCY NAME & ADDRESS(if different from Controlling Office)		15. SECURITY CLASS. (of this report) UNCLAS
		15a. DECLASSIFICATION/DOWNGRADING SCHEDULE

16. DISTRIBUTION STATEMENT (of this Report)

APPROVED FOR PUBLIC RELEASE; DISTRIBUTION UNLIMITED

DTIC
ELECTE
SEP 17 1986
B

17. DISTRIBUTION STATEMENT (of the abstract entered in Block 20, if different from Report)

18. SUPPLEMENTARY NOTES

APPROVED FOR PUBLIC RELEASE: IAW AFR 190-1

LYNN E. WOLAVER
Dean for Research and
Professional Development
AFIT/NR

19. KEY WORDS (Continue on reverse side if necessary and identify by block number)

20. ABSTRACT (Continue on reverse side if necessary and identify by block number)

ATTACHED.

DD $_{1\text{ JAN } 73}^{\text{FORM}}$ 1473 EDITION OF 1 NOV 65 IS OBSOLETE

ABSTRACT

Mesoscale Convective Complex vs. Non-Mesoscale

Convective Complex Thunderstorms:

A Comparison of Selected Meteorological Variables. (August 1986)

Michael Eugene Hoofard, A.S., San Antonio College

B.S., Texas A&M University

Chairman of Advisory Committee: Prof. Walter K. Henry

A comparative investigation of mesoscale convective complex
(MCC) and non-mesoscale convective complex (non-MCC) prestorm environ-
ments is conducted. Eleven atmospheric variables normally associated
with thunderstorm formation are either observed or calculated for a
total of nine MCC and nine non-MCC storms. These variables include:
850 mb mixing ratio, 850 mb advection of water vapor, 850 mb flux
divergence of water vapor, surface to 500 mb average relative humidity,
precipitable water, the Totals Index, the Total Energy Index, 1000-700
mb thickness advection by the 850 mb wind, 500-300 mb thickness advec-
tion by the 400 mb wind, vorticity advection at 500 mb, and vertical
velocity at 700 mb. Mean values are calculated for the eleven varia-
bles according to storm type. Then, the mean values from the MCC cases
are compared statistically with the corresponding non-MCC values.
Results show that a significant difference exists for the following
mean values: 850 mb mixing ratio, 850 mb advection of water vapor,
precipitable water, Total Energy Index, and 1000-700 mb thickness
advection. The low-level water vapor advection and thickness advection ⟶

(cont)

Variables are combined to form a low-level energy rate of change term. This energy rate of change term is found to provide an even better distinction between MCC and non-MCC storm environments.

Accession For		
NTIS GRA&I	✓	
DTIC TAB	☐	
Unannounced	☐	
Justification		
By		
Distribution/		
Availability Codes		
Dist	Avail and/or Special	
A-1		

MESOSCALE CONVECTIVE COMPLEX VS. NON-MESOSCALE CONVECTIVE COMPLEX

THUNDERSTORMS: A COMPARISON OF SELECTED METEOROLOGICAL VARIABLES

A Thesis

by

MICHAEL EUGENE HOOFARD

Submitted to the Graduate College of
Texas A&M University
in partial fulfillment of the requirements for the degree of

MASTER OF SCIENCE

August 1986

Major Subject: Meteorology

MESOSCALE CONVECTIVE COMPLEX VS. NON-MESOSCALE CONVECTIVE COMPLEX

THUNDERSTORMS: A COMPARISON OF SELECTED METEOROLOGICAL VARIABLES

A Thesis

by

MICHAEL EUGENE HOOFARD

Approved as to style and content by:

Walter K. Henry
(Chairman of Committee)

Dusan Djuric
(Member)

Ronald R. Hocking
(Member)

James R. Scoggins
(Head of Department)

August 1986

ACKNOWLEDGMENTS

Assistance from the following people helped make this investigation and report possible. I offer my sincere thanks to each one of them.

To committee chairman Prof. Henry for his foresight, overall guidance, and encouragement.

To committee members Dr. Djuric and Dr. Hocking for their technical assistance.

To my sister Sherrie for inputting computer data and typing the first draft.

To Lori and Mary Lynn for their typing assistance.

To B. J. Tiedeman for typing the final manuscript.

To my wife Judy for her support and patience.

TABLE OF CONTENTS

TABLE OF CONTENTS (Continued)

LIST OF TABLES

LIST OF FIGURES

LIST OF FIGURES (Continued)

LIST OF FIGURES (Continued)

1.   INTRODUCTION

Prior to 19/ɔ, meteorologists had recognized three basic types of thunderstorm systems. The classification scheme was based upon the storm's physical appearance and organization and depended largely upon the availability of radar observations. The three basic types are the individual air mass thunderstorm, the thunderstorm cluster, and the squall line. Of these three, the squall line displayed the greatest organization and generally covered the largest area. With the increasing use of meteorological satellites, however, a fourth type has been observed. Referred to as a mesoscale convective complex (MCC), this storm type is similar to the squall line in that it covers large areas and appears highly organized. However, its nearly circular shape as depicted in satellite imagery readily distinguishes it from the elongated squall line.

Primarily nocturnal in nature, MCCs have been observed over the United States during the months of March through September. Climatological studies for the United States (Maddox, 1981; Maddox et al., 1982; Rogers and Howard, 1983) indicate an average occurrence of 33 storms per season. Of the 131 MCCs documented, 46 percent produced tornadoes, 58 percent produced hail, and 65 percent produced damaging winds. In addition, flooding occurred with 36 percent of the storms.

Because of the MCCs destructive potential, interest in forecasting these intense convective storms has developed quickly. Unfortunately, numerical models presently in operation have not provided

---

Citations follow the style of the Monthly Weather Review.

adequate guidance (Maddox, 1981). Their inadequacy should not be surprising, however. The problem plaguing any thunderstorm forecast is the dependence upon synoptic scale data to predict a mesoscale event. To complicate matters, forecasters attempt to predict not only thunderstorm occurrence but the level of severity as well. Now, with the goal of forecasting MCCs, meteorologists face an even more demanding problem. Can the atmospheric environment leading to MCC formation be distinguished from that leading to other types of convective storms, severe or otherwise? While experiments in forecasting MCCs have been undertaken, no one has addressed this question directly. This investigation is a beginning venture to answer this question.

2.   LITERATURE REVIEW OF THE MCC

MCCs were first detected and recognized as unique storm systems during the mid 1970s through the use of geosynchronus satellite imagery. Figure 1 depicts a typical enhanced infrared (IR) image of the MCC while Fig. 2 shows the corresponding radar echo. The formal definition of the MCC was developed solely from enhanced IR observations and is reproduced in Table 1.

Maddox (1981), in his dissertation, completed the first comprehensive investigation of these storms. His work included a brief climatology of MCCs, an objective analysis of the meteorological conditions spanning their life-cycle, the development of a physical model of the MCC, and an introductory investigation of the storm's moisture and kinetic energy budgets. He found the following features to precede persistently the genesis of these convective systems: 1) an approaching weak, mid-tropospheric short-wave trough, 2) strong low-level warm advection, 3) a conditionally unstable atmosphere, 4) a significant east-west moisture gradient, and 5) the presence of a frontal zone. Additional studies by Maddox et al. (1981) dealt with the effects of the MCC on its environment. They concluded that the mesoscale, convectively driven circulation significantly alters upper-tropospheric environmental conditions, particularly temperature, height, and wind fields.

MCC precipitation studies by Fritsch et al. (1981) showed the beneficial aspect of these storm systems. MCCs were found to produce rainfall over large areas and to account for a significant portion of the rainfall during the growing season over much of the corn and wheat
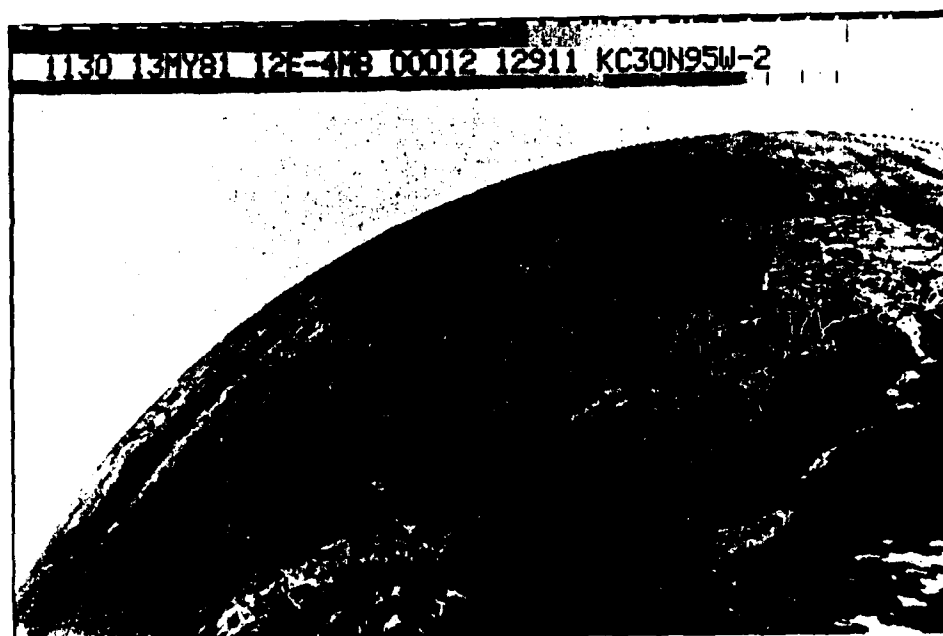
Fig. 1. Enhanced infrared satellite image for 1130 GMT 13 May 1981. MCC identified by large, black region centered over Missouri (after Maddox et al., 1982).

Fig. 2. Section of National Weather Service radar summary chart for 1135 GMT 13 May 1981.

Table 1. Definition of mesoscale convective complex (after Maddox, 1981).

Physical characteristics

Size:	A: Cloud shield with IR temperature $\leqslant$ -32°C must have an area $\geqslant$ 100,000 km^2 B: Interior cold cloud region with temperature $\leqslant$ -52°C must have an area $\geqslant$ 50,000 km^2
Initiate:	Size definitions A and B are first satisfied
Duration:	Size definitions A and B must be met for a period of $\geqslant$ 6 h
Maximum extent:	Contiguous cold cloud shield (IR temperature $\leqslant$ -32°C) reaches maximum size
Shape:	Eccentricity (minor axis/major axis) $\geqslant$ 0.7 at time of maximum extent
Terminate:	Size definitions A and B no longer satisfied

belts of the United States.

Wetzel et al. (1982) investigated the dynamic structure of several MCCs. They then compared the MCCs' vertical profiles of divergence to those from tropical cloud clusters and a typical mid-latitude cyclone. Finally, they compared the MCCs' and cyclone's vertical profiles of average meridional sensible heat transport. Results suggest that the MCC develops in a highly barotropic environment and, thus, is driven basically by convective instability.

Cotton et al. (1983) and Wetzel et al. (1983), using data collected during the South Park Area Cumulus Experiment, investigated the evolution of MCCs from mountain generated convective cells over

Colorado. They concluded that a mid-latitude MCC is similar to its tropical counterpart in that their dynamics are essentially controlled by buoyant instability. Thus, they suggested that the weak baroclinic zones often located near developing MCCs "act primarily to trigger and direct the release of buoyant instability." Cotton et al. further hypothesized that as baroclinicity increases, convection will tend to favor the typical squall line structure rather than the elliptical shape characteristic of MCCs.

During the summers of 1982 and 1983, experiments in forecasting the MCC were conducted jointly by personnel at the Environmental Research Laboratory in Boulder, Colorado, and at the Satellite Field Service Station in Kansas City, Missouri. A summary of the 1982 experiment was presented at the American Meteorological Society's 13th Conference on Severe Local Storms (Maddox et al., 1983). During this first summer, a total of 117 forecasts were made with the following results: 20 forecasts for MCC occurrence verified, 58 forecasts for no occurrence verified, 31 forecasts for MCC occurrence did not verify, and 8 MCC events were not forecast. The false alarm ratio, the number of times the event was forecast but did not occur divided by the total number of times the event was forecast, was 0.61. Distinguishing differences between the synoptic conditions leading to MCCs and those resulting in non-MCC thunderstorms proved to be a difficult task.

3. OBJECTIVE

The effects of the MCC on man and his environment have been both harmful and beneficial. Consequently, the National Oceanic and Atmospheric Administration has given high priority to the development of operational MCC forecast procedures and techniques. The primary objective of this research is to determine if MCC and non-MCC prestorm environments can be distinguished from one another using routine synoptic data. To accomplish this goal, a comparative investigation of MCC to non-MCC convective storms was performed.

4. INVESTIGATIVE PROCEDURE

In conducting this comparative investigation, selected meteorolo-
gical variables were either observed or calculated for a total of nine
MCC and nine non-MCC storms. Mean values were then determined for each
variable. The mean values derived from the MCC cases were compared
statistically with the corresponding non-MCC values to determine if a
significant difference existed. The following sections outline this
procedure in greater detail.

a. Selection of Meteorological Variables

Thunderstorm formation depends upon the availability of
sufficient water vapor, unstable air, and a triggering mechanism.
These three requirements guided the selection of the meteorological
variables. A summary of the variables selected is provided in Table 2.

Table 2. Meteorological variables selected for evaluation of MCC and
non-MCC storms.

1. 850 mb mixing ratio
2. 850 mb advection of water vapor
3. 850 mb flux divergence of water vapor
4. Surface-to-500 mb average relative humidity
5. Precipitable water
6. Totals Index
7. Total Energy Index
8. 1000-700 mb thickness advection by 850 mb wind
9. 500-300 mb thickness advection by 400 mb wind
10. Vorticity advection at 500 mb
11. Vertical velocity at 700 mb

(1) Water vapor

By mass, approximately one half of the atmosphere's water vapor is located below 800 mb. Palmen and Newton (1969) have estimated that for a large intense thunderstorm, about 90 percent of the inflow water vapor enters near the base of the updraft. Sienkiewicz (1981), in her moisture budget study of convective activity, "found horizontal moisture convergence to be the dominant term within the 900-750 mb layer." Maddox (1981) observed similar results in his investigation of ten MCCs. Consequently, low-level water vapor measurements and processes have been stressed in this study. The 850 mb mixing ratio observations were used to obtain an instantaneous measure of available water vapor; 850 mb water vapor advection and flux divergence were calculated to determine changes occurring within the moisture field.

A question raised during this research concerned the adequacy of the 850 mb mixing ratio in representing low-level water vapor content. More specifically, how often might a moist surface layer go unrecognized due to the capping effect of an inversion below the 850 mb surface? The mean mixing ratio of the lowest 100 mb is a more representative value of low-level water vapor content but it is not readily available. To determine if the 850 mb data adequately depicted the presence of low-level humidity, a comparison was made. Dewpoint depressions at the 850 mb level were compared against the corresponding surface values for each storm case selected. For the MCC data, 16 percent of the observations had 850 mb dewpoint depressions more than $3^{\circ}C$ larger than the corresponding surface values. For the non-MCC data, a value of 13 percent was found. In both cases, Gulf coastal

stations accounted for approximately 45 percent of the dewpoint depression variations. None of the storm cases used in this research, however, occurred within 550 km of the coast. Based upon these findings, the 850 mb mixing ratio was accepted as a sufficiently accurate indicator of low-level humidity.

Surface-to-500 mb average relative humidity and precipitable water were selected as additional indicators of available water vapor. These two, however, include the added effect of middle and upper-level water vapor. Maddox (1983) found MCCs to form near precipitable water maxima.

(2) Stability

Both conditional and convective stabilities play important roles in the promotion of convection. If the environmental lapse rate lies between the dry and moist adiabatic lapse rates, the atmosphere is said to be conditionally unstable. With sufficient lifting, a parcel of air becomes saturated and eventually buoyant with respect to its surroundings. Often, however, soundings which are conditionally unstable in the lower levels may exhibit capping inversions at higher levels. Unless the inversion is removed, convection will be inhibited. If the equivalent potential temperature within the inversion layer decreases with height, upward displacement of the layer will result in destabilization and, thus, destroy the inversion. Layers of the atmosphere in which the equivalent potential temperature decreases with height are said to be convectively unstable.

Various indices have been developed to depict the degree of atmospheric instability. In general, these indices yield similar

results, especially for a warm, moist air mass (Miller, 1967). Two indices selected for this study are the Totals Index and Total Energy Index. A study of the 1964 and 1965 tornado events revealed that 92 percent of the storms were characterized by a Totals Index of 50 or greater (Miller, 1967). The Total Energy Index, which is based upon the vertical variation in static energy, has also proved useful in identifying severe storm threat areas. Darkow (1968) found total energy values to be significantly higher for soundings near tornadic storms. In addition, he maintains that the index holds a slight advantage over the Showalter and Lifted indices through its ability to account for contributions of cold mid-tropospheric air. Intrustions of cold, upper-level air appear to play an important role in the total energy release of severe convective storms. Tables 3 and 4 show the guidance provided for applying the Totals and Total Energy indices.

(3) *Triggering actions*

The presence of abundant water vapor and potentially unstable layers does not ensure the development of thunderstorms. Unless some mechanical process induces upward vertical motion, the potential instability will not be released. Triggering actions evaluated in this study include low-level warm advection, upper-level cold advection, and positive vorticity advection.

The quasi-geostrophic omega equation is useful for diagnosing vertical motion fields within the large scale baroclinic environment. Qualitatively, *air rises in regions where either differential vorticity advection or low-level warm advection is occurring* (Holton, 1972). Quantitative assessment is difficult, however, since the differential

Table 3. Suggested guidance for using the Totals Index (after Miller, 1967).

Totals Index Value	Interpretation
44	isolated thunderstorms
46	scattered thunderstorms; some heavy
48	scattered thunderstorms; some heavy and isolated severe
50	scattered heavy thunderstorms, some severe
52	scattered to numerous heavy thunderstorms; some severe with tornadoes possible
56	numerous heavy thunderstorms; scattered severe thunderstorms with tornadoes

Table 4. Suggested guidance for using the Total Energy Index (after Darkow, 1968).

Total Energy Index Value	Interpretation
0.0 to -1.0	thunderstorms possible; not severe
-1.0 to -2.0	thunderstorms; isolated severe
less than -2.0	severe thunderstorms; tornadoes likely

vorticity advection term and temperature advection term often imply
vertical motions of opposite sign. Studies of the MCC prestorm
environment (Maddox, 1983) generally indicate the presence of strong
warm advection below 700 mb but quite weak PVA aloft. These findings
suggest that the vertical motion preceding MCC development is induced
primarily by warm advection.

The validity of applying the omega equation to the MCC environ-
ment is questionable, however. Foremost, findings from earlier
investigations tend to classify the MCC environment as barotropic in
spite of the storm's usual proximity to a surface front and advancing
short-wave trough. But even if the environment can be classified as
baroclinic, the proximity to a surface front raises scaling questions.
Derived for the diagnosis of mid-latitude synoptic scale motions, the
omega equation does not include the vertical advection and twisting
terms of vorticity. These terms are often important in the vicinity
of atmospheric fronts (Holton, 1972). Thus, because the MCC prestorm
environment often includes a surface front, the omega equation may not
be applicable.

The quantitative relationship between low-level warm advection
and the vertical motion field associated with developing MCCs is still
unknown. The destabilizing effect of warm advection and its relation-
ship to severe convective activity has been observed for many years,
however. As early as 1952, MacDonald related lower-tropospheric warm
advection to the formation and maintenance of squall lines. Recently,
Hales (1982) demonstrated the predominance of strong warm advection at
both 850 and 700 mb during tornado events. The close relationship

which has been observed between warm advection and severe, organized convection warrants its selection as a possible triggering action.

Since cold advection aloft also results in atmospheric destabilization, it too will be evaluated as a triggering action. Crawford (1950) noted the common occurrence of cold advection aloft during the formation of pre-frontal thunderstorms. He demonstrated cases of differential advection in which the cold, upper-level trough moved eastward faster than the low-level warm sector. Fulks (1951) made similar observations in his study of the instability line. Rhea (1966) noted that thunderstorms often formed along dry lines when supported by cold advection aloft. Since cold pockets aloft are usually associated with troughs and minor short-waves, it may be technically more appropriate to classify cold advection as an indicator rather than an actual trigger (Palmen and Newton, 1969). Thus a dynamical triggering process needs to be considered as well.

Basic dynamic theory depicts rising air downstream of upper-level troughs and descending air downstream of upper-level ridges. The presence of these vertical motion fields is often explained in terms of vorticity advection. On the synoptic scale, PVA downstream of the trough generally implies the presence of convergence below the level of nondivergence and divergence above. Thus, the upward vertical motion field is established. Miller (1967) ranked vorticity advection as the most important variable related to severe weather out-breaks. Although more recent studies (Hales, 1979; Maddox and Doswell, 1982) downplay the importance of PVA at 500 mb, it was selected as a triggering action to be evaluated.

(4) Vertical motion

Sustained upward motion is critical to the formation and persist-
ence of thunderstorm activity. In general, the stronger the upward
velocity, the more favorable an area will be for thunderstorm forma-
tion. Vertical velocity was the final meteorological variable examined
for its value in distinguishing between MCC and non-MCC prestorm
environments.

b.   Data Sources

Values for the selected variables were determined using either
National Meteorological Center (NMC) facsimile charts or the mandatory
level sounding data. Precipitable water and surface-to-500 mb average
relative humidity data came directly from the NMC charts. Vertical
velocity was estimated using the LFM 12-24 h forecast charts.
Vorticity advection was estimated using the 500 mb Height/Vorticity
Analysis chart. The remainder of the variables were either obtained
directly or computed from the sounding data. Storm locations were
identified using radar facsimile charts. For informational purposes,
NMC surface charts were reviewed to identify frontal locations.

c.   Case Selection Criteria

Because sounding data were available only for those stations
identified in Fig. 3, storms occurring outside this domain or along
its borders were not considered. MCC and non-MCC selection criteria
differed somewhat; MCC selection is discussed first. Only those MCCs
identified in the 1981 and 1982 annual summaries (Maddox et al., 1982;
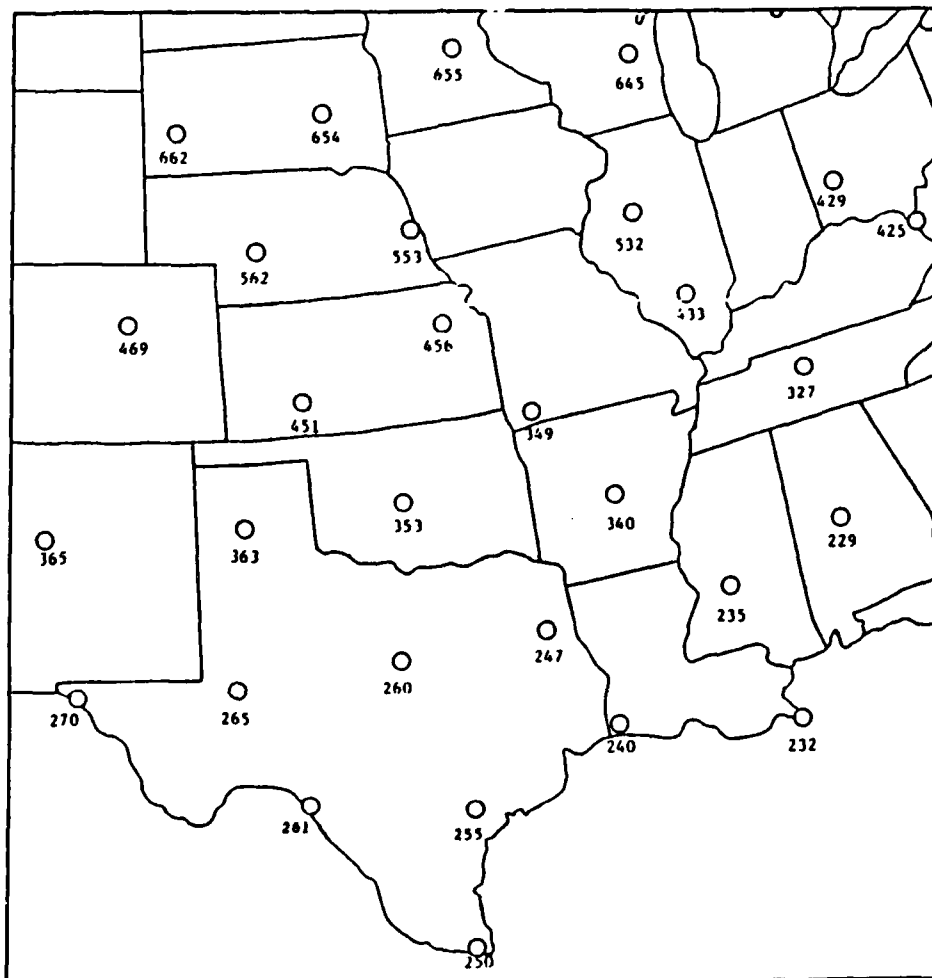
Fig. 3. Stations from which upper-air sounding data were used.

Rogers and Howard, 1983) were considered. Thus, the storms selected
as MCCs had already been verified as meeting the formal criteria used
to define the MCC. These summaries listed both the time in which the
first storms occurred and the time in which the system was classified
as an MCC. Only those systems with first storms occurring after 0000
GMT but before 1200 GMT were selected. As noted in the literature
review, the MCC has been found to alter the surrounding upper-
tropospheric environmental conditions. Since this investigation
emphasizes the pre-storm environment, an attempt was made to exclude
or at least minimize possible storm impacts. The annual summaries
indicate that approximately 75 percent of the MCCs develop between
0000 and 1200 GMT; over 50 percent develop between 0000 and 0600 GMT.
Using 0000 GMT sounding data and selecting storms occurring after this
time maximized the number of cases available in the late prestorm
stage. To limit the amount of elapsed time between the 0000 GMT
sounding and the time of MCC formation, no MCCs forming later than
1200 GMT were considered; 1200 GMT sounding data were avoided due to
the greater possibility of low-level inversions and unrepresentative
humidity values at 850 mb. The 1200 GMT data were used in one case.
For the 18 July 1982 MCC, the preceding 1200 GMT surface-to-500 mb
relative humidity and precipitable water charts were substituted in
place of the missing 0000 GMT data. Comparison of the substitute
chart with that available 24 hours later showed little change of
patterns. Thus, the morning sounding prior to the storm was deemed a
representative replacement. Ten cases were identified using these

criteria; however, one had to be omitted due to missing data. Table 5 lists the nine MCC events selected.

Table 5. Times and dates of storms investigated.

MCC Cases	Non-MCC Cases
1. 0735 GMT 13 May 1981	0735 GMT 16 May 1979
2. 0835 GMT 7 June 1982	0635 GMT 30 May 1979
3. 1035 GMT 8 June 1982	0635 GMT 8 June 1978
4. 0635 GMT 10 June 1981	0735 GMT 24 June 1979
5. 1035 GMT 22 June 1981	0635 GMT 11 July 1978
6. 0635 GMT 18 July 1982	0735 GMT 16 July 1979
7. 0935 GMT 23 July 1981	0835 GMT 31 July 1978
8. 0835 GMT 15 August 1982	0435 GMT 9 August 1978
9. 0535 GMT 2 September 1982	0835 GMT 2 September 1978

Selection of non-MCC cases was more complicated. To ensure that the non-MCC storms were independent of the MCC cases selected, 1981 and 1982 storm data were not considered. However, the problem of separating non-MCC storm environments still remained. To resolve this problem, MCC annual summaries (Maddox, 1981) for 1978 and 1979 were reviewed. For this two-year period, an attempt was made to select non-MCC storms occurring at least 24 h before or after an MCC event. All except one of the cases eventually chosen met this requirement. The exception occurred approximately 21 h after an MCC but was included to increase the number of non-MCC cases. Since 0000 GMT data were used for the non-MCC cases as well, selection of storms forming between 0000-1200 GMT was preferred. However, in order to obtain a sufficient

number of non-MCC cases, storms which formed prior to 0000 GMT but showed development and intensification during the preferred time period were accepted. Table 5 also lists the nine non-MCC cases selected.

d.   Evaluation of Computed Variables

For each case, sounding data from the rawinsonde station network were entered into a computer. Corresponding 850 and 500 mb mixing ratio, surface-to-500 mb relative humidity, and precipitable water data had to be entered as well. Thickness values were determined from the raw data for both the 1000-700 and 500-300 mb layers. In addition, the 850 and 400 mb wind speeds were converted from kt to km h^{-1} and separated into u and v components.

The Totals Index (TI) was calculated for each station as shown by

$$TI = (TD_{85} - T_{50}) + (T_{85} - T_{50}) \qquad (1)$$
$$= TD_{85} + T_{85} - 2 T_{50}$$

where TD_{85}, T_{85}, and T_{50} are the 850 mb dewpoint, 850 mb temperature, and 500 mb temperature in ^{o}C.

The Total Energy Index was calculated using the two-step procedure shown in (2) and (3). First, the total static energy (TE) per unit mass was determined for both the 850 and 500 mb levels by

$$TE = .24(T + 2.5w + 9.8z). \qquad (2)$$

For the specified pressure level, T is the temperature in ^{o}K, w is the mixing ratio in $g\ kg^{-1}$, and z is the height in km. Units for TE are $cal\ g^{-1}$. See Darkow (1968) for details concerning the development of this equation. By subtracting the 850 mb static energy total from the 500 mb value, the Total Energy Index is obtained.

$$TEI = TE_{50} - TE_{85} \tag{3}$$

At this point, Barnes' objective analysis (Barnes, 1964) was applied to interpolate the following station data to a grid: 1) 850 mb mixing ratio, 2) surface-to-500 mb relative humidity, 3) precipitable water, 4) Totals Index, 5) Total Energy Index, 6) u and v components of the 850 and 400 mb wind, and 7) thickness values for the 100-700 and 500-300 mb layers. The grid was designed for use with the NMC radar facsimile chart. This feature allowed direct comparison of analyzed fields to the associated storm echoes. The grid is illustrated in Fig. 4; grid spacing is 250 km at 40° north latitude.

Upon completion of the interpolation scheme, grid values had been determined for five of the eleven selected variables. The gridding technique was not used in estimating vorticity advection or vertical motion. However, grid values were required for these remaining variables: 1) low-level warm advection, 2) upper-level cold advection, 3) 850 mb advection of water vapor, and 4) 850 mb flux divergence of water vapor. The computations of these variables are discussed below.

Temperature advection in the desired layers was determined in terms of thickness advection. Low-level thickness advection was
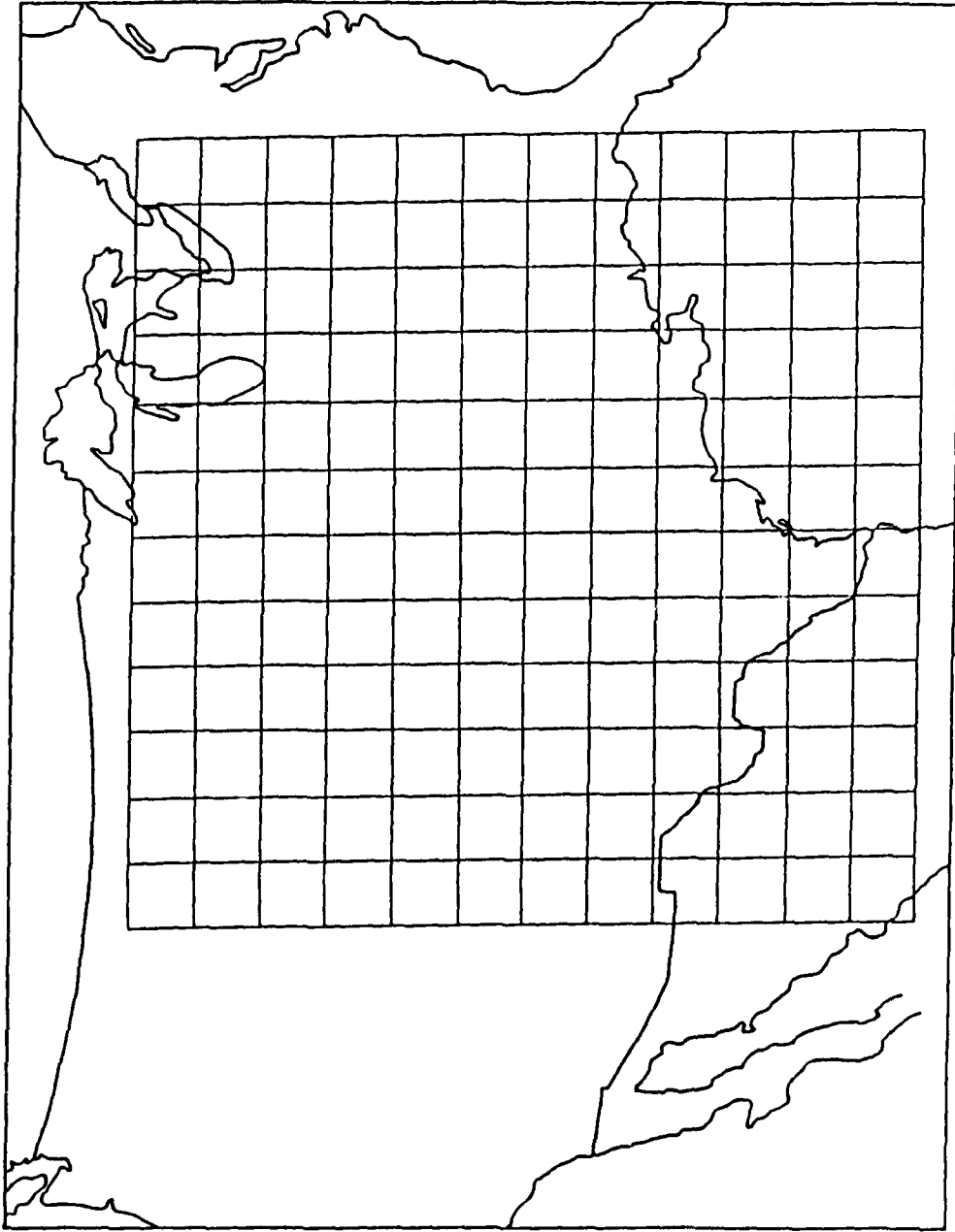
Fig. 4. Grid used for objective interpolation of sounding data; spacing is 250 km.

estimated using the 1000-700 mb thickness and the 850 mb wind. Upper-
level thickness advection was estimated using the 500-300 mb thickness
and the 400 mb wind. Thickness advection values were calculated for
the center of each grid box. Advection by the u and v wind components
was calculated separately and then added to obtain the total advection.
Equations (4), (5), and (6) in combination with Fig. 5 illustrate the
computational method employed.

Fig. 5. Sample grid box with location of variables used for
thickness advection calculation.

Thickness advection by u:

$$-u \frac{(\partial \Delta\phi)}{\partial x} = \left[\frac{-(u_1 + u_2 + u_3 + u_4)}{4} \right] \left[\frac{(\Delta\phi_2 + \Delta\phi_4) - (\Delta\phi_1 + \Delta\phi_3)}{2\Delta x} \right] \quad (4)$$

Thickness advection by v:

$$-v \frac{(\partial \Delta\phi)}{\partial y} = \left[\frac{-(v_1 + v_2 + v_3 + v_4)}{4} \right] \left[\frac{(\Delta\phi_1 + \Delta\phi_2) - (\Delta\phi_3 + \Delta\phi_4)}{2\Delta y} \right] \quad (5)$$

Total advection:

$$\qquad\qquad (A) \qquad (B)$$
$$-\vec{V}\cdot\nabla(\Delta\phi) = -\left[u\frac{(\partial \Delta\phi)}{\partial x} + v\frac{(\partial \Delta\phi)}{\partial y} \right] \qquad (6)$$

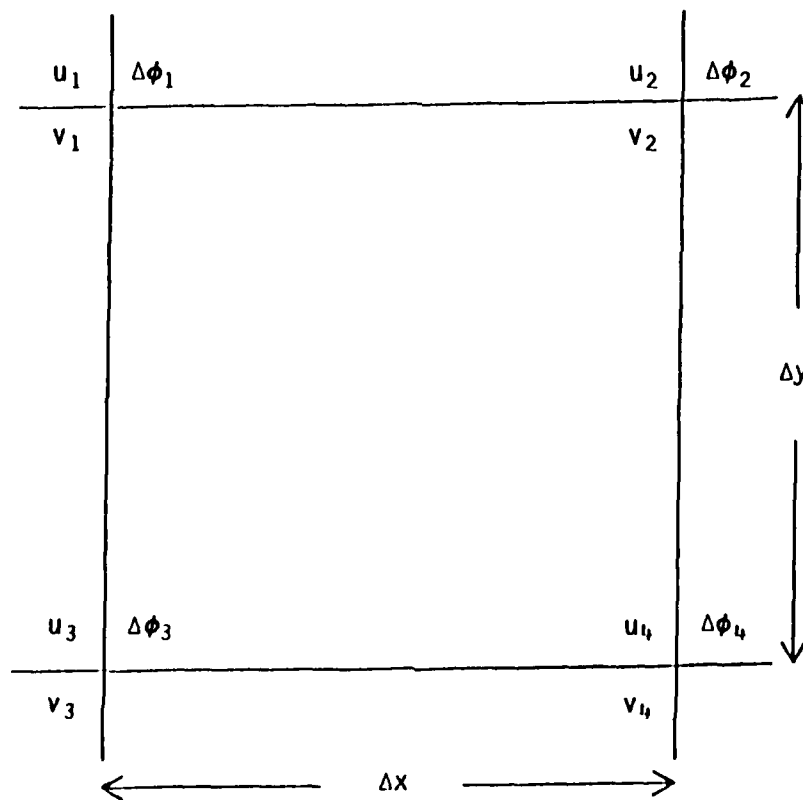where terms A and B represent the values of expressions (4) and (5), respectively. For these and the following calculations, units for x and y, u and v, and ϕ are km, km h^{-1}, and gpm. Resulting units for thickness advection are gpm h^{-1}.

Computation of the advection of water vapor at 850 mb was performed in a similar manner. The substitution of mixing ratio (w) for thickness ($\Delta\phi$) was the only change required before using (4), (5), and (6). Units are g kg^{-1} for w and g kg^{-1} h^{-1} for the advection of water vapor.

Flux divergence of water vapor at 850 mb was calculated using (7). Like the advection values, it was determined for the center of each grid box. For all computations involving water vapor, the mixing ratio has been substituted in place of the specific humidity (q).

$$w\nabla\cdot\vec{V} = \frac{(w_1+w_2+w_3+w_4)}{4} \left[\frac{(u_2+u_4)-(u_1+u_3)}{2\Delta x} + \frac{(v_1+v_2)-(v_3+v_4)}{2\Delta y} \right] \qquad (7)$$

Resulting units for the flux divergence of water vapor are g kg^{-1} h^{-1}. The total flux divergence, $\nabla\cdot(w\vec{V})$, was not included among the variables to be investigated. Maddox's (1981) investigation of ten MCCs showed little numerical difference between vapor flux divergence and total vapor flux divergence in the MCC prestorm environment.

e.   Evaluation of Gridded Fields

Using the processing and computational procedures discussed above, grid values were computer produced for the first nine variables listed in Table 2. Thus, nine fields were obtained for each MCC and non-MCC case. Although each field was drawn by hand, the exact location of the associated storm was not identified before completing the analysis. This technique was used to promote analysis objectivity.

To determine the variables associated with each storm, each analyzed chart was positioned over the corresponding radar facsimile chart. Radar echoes better depicted the MCC's region of strong, active convection and, thus, were chosen over enhanced IR satellite imagery. While each analyzed chart was based on 0000 GMT data, the corresponding radar chart was based on a radar observation taken sometime between 0000-1200 GMT. For each MCC case, the actual observation selected was the one taken closest to the time of MCC formation. As mentioned earlier, the formation times were available within the MCC annual summaries. In general, the radar chart selected for a non-MCC

case was one depicting storm development and intensification. A
series of charts for the MCC and non-MCC conditions are shown in
Appendix A. Radar echoes not a part of the MCC or non-MCC storm
system are not shown.

After superimposing each set of isopleths over the correspond-
ing storm radar echo, representative values were determined using the
following rules.

1) Only values occurring within the echo region were considered.

2) The largest 850 mb mixing ratio, surface-to-500 mb relative
humidity, and precipitable water values were recorded.

3) The largest positive value of 850 mb water vapor advection
was recorded; if the echo region contained no positive values, the
smallest advection value was recorded.

4) The largest value of 850 mb water vapor flux convergence was
recorded; if the echo region contained no convergence values, the
smallest value of water vapor flux divergence was recorded.

5) The Totals Index and Total Energy Index values representing
the greatest instability were recorded.

6) The largest positive value of low-level thickness advection
was recorded; if the echo region contained no positive values, the
smallest advection value was recorded.

7) The largest negative value of upper-level thickness advection
was recorded; if the echo region contained no negative values, the
smallest advection value was recorded.

Certain limitations and biases were inherent to this evaluation
procedure. Time differences between the analyzed fields and the

corresponding radar echoes limited the representativeness of the recorded values. This limitation was not considered a major problem, however, because of generally light mid-level steering winds and a relatively large grid spacing (250 km). In other words, storm movement between 0000 GMT and the time of the radar depiction was normally less than one grid space. The procedure for selecting largest and smallest values produced biased results. The values favorable to thunderstorm development were maximized while those unfavorable were minimized. Since this technique was applied to both MCC and non-MCC cases, the bias was not considered detrimental to the investigation. The flexibility of this technique helped compensate for the time limitation discussed above and, thus, aligned results more closely with theory. The use of extreme rather than average values was important for another reason as well. The identification of a mesoscale disturbance within a synoptic network is more likely when using data extremes instead of averages.

f. Estimation of Vorticity Advection

Vorticity advection estimates were obtained for each case using 0000 GMT NMC 500 mb Height/Vorticity Analysis charts. After enlarging the charts, they were altered to include 30 m contour intervals. The MCC and non-MCC echoes as depicted on the radar charts were transferred to the corresponding height/vorticity charts. Echo selection times were the same as those discussed in section 4e. On each NMC analysis, a square box with sides of 500 km (2 grid spaces) was drawn upstream from the radar echo as indicated by the contours. The storm center
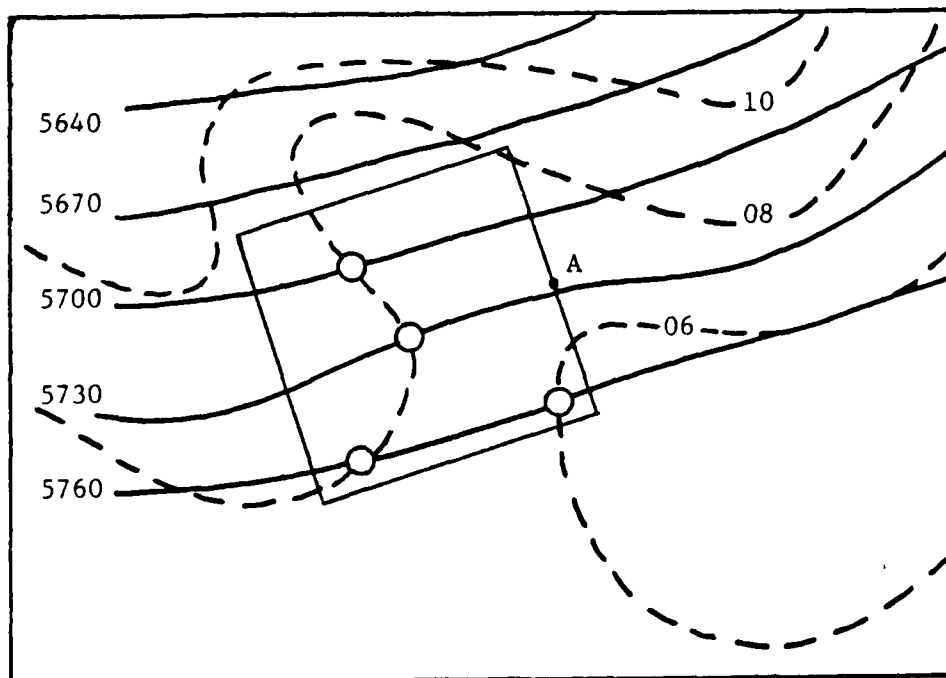
Fig. 6. Illustration of technique for estimating vorticity advection. Solid lines are 500 mb height contours in gpm. Dashed lines are isolines of vorticity ($X10^{-5}s^{-1}$). Point A represents the storm center. Height contour and vorticity isoline intersections within the box are highlighted by circles. For this example, the boxed region is characterized by PVA with four intersections.

was located at the midpoint of the box's downstream end. This downstream end was positioned normal to the contours. Figure 6 illustrates such a box. The area within each box was then classified according to the type of vorticity advection. Thus, the boxes represented areas of either positive, negative, or neutral vorticity advection. The intensity of the PVA or NVA was evaluated by counting the number of height contour and vorticity isoline intersections. A larger number of intersections implies stronger PVA or NVA. This procedure provided

a quick field method for evaluating the type and intensity of vorticity advection associated with each storm.

g.   Estimation of Vertical Motion

The LFM provides 12-48 h vertical velocity forecasts for the 700 mb level. Isolines of vertical motion are drawn in intervals of 2 μb s^{-1} beginning with the + 0 line. The 12 and 24 h forecasts valid at 0000 and 1200 GMT were used to infer synoptic scale vertical motions associated with each storm. A single value for vertical velocity was interpolated using both charts since the time of storm occurrence varied between 0000-1200 GMT. Estimates were made to the nearest μb s^{-1}.

h.   Statistical Evaluation

Once the variables had been obtained for each storm, mean values were calculated for the MCC and non-MCC cases. Then, the MCC mean values were compared statistically against their non-MCC counterparts to determine if a significant difference existed. Assuming independence and equal but unknown variances, the hypothesis that the corresponding MCC and non-MCC mean values were not significantly different was tested using the Student t test. The test statistic for testing the equality of means is shown by

$$t = (\bar{X}_1 - \bar{X}_2)/[S^2(1/n_1 + 1/n_2)]^{1/2} \tag{8}$$

where $\bar{X}_1$ and $\bar{X}_2$ are the mean values for each test group, S^2 is the estimate of the common variance, and n_1 and n_2 are the number

of observations from each group. S^2 is calculated using

$$S^2 = [(n_1 - 1)S_1^2 + (n_2 - 1)S_2^2]/(n_1 + n_2 - 2). \tag{9}$$

Again, n_1 and n_2 are the number of observations from each test

group while S_1^2 and S_2^2 are the sample variances for each test

group.

Once the test statistic for each pair of mean values was com-

puted, it was checked against the appropriate critical region found in

a cumulative t distribution table. If the test statistic was located

within the acceptance region for a specified significance level, the

hypothesis of equality was accepted and the two means were considered

to come from the same population. If the test statistic was located

outside of this region, however, the hypothesis was rejected and the

two means were considered to come from different populations. When

testing the equality of two means, the acceptance region is defined

by the interval

$$\pm\ t\ (1-\alpha/2)(n_1+n_2-2) \tag{10}$$

where α represents the significance level. The significance level is

the probability of rejecting a hypothesis that is actually correct.

For this investigation, however, a particular significance level was

not specified. Instead, the significance level at which rejection

first occurred was recorded. Only levels between 0 and .50 were

considered.

This statistical analysis was based on a total of nine MCCs and

nine non-MCCs. The small sample size is recognized as an investigative

weakness since statistical reliability is lessened. Currently, a relaxation in case selection criteria would be required to increase the MCC sample size. As more MCC annual summaries become available, the sample size problem will diminish.

5. ERROR DISCUSSION

Fuelberg (1974) has estimated the root mean square (RMS) errors associated with upper-air measurements. His results are shown in Table 6. Based upon his data, errors have been estimated for the observed and computed variables used in this study. Table 7 lists the RMS errors determined for each parameter. Fuelberg's estimate of humidity error was applied directly to the first three variables.

The errors for the stability indices were estimated using the following procedure. Values from (1) and (3) were calculated using typical estimates for the right-hand side quantities. Thus, a typical value was obtained for the two indices. The right-hand side quantities were then altered by an amount equal to the respective RMS errors found in Table 6. Care was taken at this step to ensure that the inserted errors would be additive rather than compensating. Using these adjusted quantities, the values were recalculated. The difference between the first and second solution for each index represented an estimate of the RMS error.

RMS errors for advection and flux divergence computations were estimated in basically the same manner. Using equations (4) through (7) and grid point values from data fields obtained in this research, advection and divergence were computed. After this calculation, all of the quantities at a single grid point were altered by an amount equal to their respective RMS errors. Again, care was taken to ensure the inserted errors would be additive. The solution was then recalculated. As before, the difference from the original solution represented the error estimate. This procedure was conducted

Table 6. Estimated root mean square errors associated with upper-air measurements (after Fuelberg, 1974).

Parameter	Pressure Level	Approximate RMS Error
Temperature	---	0.5°C
Pressure	surface to 400 mb	1.3 mb
	400 to 100 mb	1.1 mb
	100 to 10 mb	0.7 mb
Humidity	---	10%
Pressure altitude	500 mb	10 gpm
	300 mb	20 gpm
	50 mb	50 gpm
Wind speed	700 mb	0.5 m s^{-1} for 40° elevation
		2.5 m s^{-1} for 10° elevation
	500 mb	0.8 m s^{-1} for 40° elevation
		4.5 m s^{-1} for 10° elevation
	300 mb	1.1 m s^{-1} for 40° elevation
		7.8 m s^{-1} for 10° elevation
Wind direction	700 mb	1.3° for 40° elevation
		9.5° for 10° elevation
	500 mb	1.8° for 40° elevation
		13.4° for 10° elevation
	300 mb	2.5° for 40° elevation
		18.0° for 10° elevation

Table 7. Estimated root mean square errors for selected variables.

Variable	RMS Error
850 mb mixing ratio	10%
Surface-to-500 mb average relative humidity	10%
Precipitable water	10%
Totals Index	2
Total Energy Index	1.0 cal g^{-1}
850 mb water vapor advection	0.13 g kg^{-1} h^{-1}
850 mb flux divergence of water vapor	0.05 g kg^{-1} h^{-1}
1000-700 mb thickness advection	0.6 gpm h^{-1}
500-300 mb thickness advection	3.0 gpm h^{-1}

separately for all four grid points to determine the maximum error. The entire procedure was then repeated for several grid boxes to obtain an average maximum error.

Table 7 represents only those errors caused by the accuracy limitations of meteorological instruments. Errors introduced through the use of the gridding scheme were not considered. Regardless, the RMS error estimates provided should still be useful when evaluating the reliability of investigative results. Because vorticity advection and vertical velocity were approximated from precalculated values instead of observed values of instruments, the RMS errors were not estimated.

6.   RESULTS

a.   Statistics

Samples of the charts depicting prestorm fields are contained in
Appendix A. Figures A-1a through A-1k illustrate the fields associated
with the 15 August 1982 MCC. Figures A-2a through A-2k are similar but
for the 9 August 1978 non-MCC storm. Table 8 summarizes the informa-
tion obtained from the eighteen storm cases. It lists the range and
mean value of each variable for the two storm categories.

By comparing these MCC and non-MCC values, several differences
can be seen. Looking at the range column first, note that considerable
overlap occurs with each variable. While the most favorable values for
strong convection are associated predominantly with the MCC, this is
not always the case. The non-MCC category has a higher value of 850 mb
water vapor flux convergence and a higher Totals Index value. Its
maximum value for surface-to-500 mb average relative humidity equals
that of the MCC column. On the opposite end of the scale, those
values least favorable for convection are generally associated with the
non-MCCs, vorticity advection and forecast vertical velocity being the
only exceptions.

Referring to the mean value column, a few more relationships are
evident. While there are no sign differences between the correspond-
ing MCC and non-MCC values, the MCC mean value in every category is
more conducive to convection. For the vapor variables, two important
differences should be noted. First, the water vapor content of the MCC
prestorm environment is 23 percent greater than that for the non-MCC

Table 8. Variable range and mean value for MCC and non-MCC cases.

Variable	Range		Mean Value	
	MCC	non-MCC	MCC	non-MCC
850 mb mixing ratio (g kg^{-1})	10.0 to 16.5	6.0 to 15.0	13.6	11.0
850 mb advection of water vapor (g kg^{-1} h^{-1})	0 to +.40	-.05 to +.21	+.20	+.06
850 mb flux divergence of water vapor (g kg^{-1} h^{-1})	-1.07 to +.10	-1.20 to +.40	-.46	-.25
Surface-to-500 mb average relative humidity (%)	50 to 70	40 to 70	59	57
Precipitable water (inches)	.95 to 1.90	.85 to 1.60	1.52	1.23
Totals Index	48 to 56	46 to 58	52	50
Total Energy Index (cal g^{-1})	-1.5 to -6.0	+0.4 to -4.5	-3.7	-2.5
1000-700 mb thickness advection (gpm h^{-1})	0 to +6.0	-0.5 to +2.0	+2.5	+0.7
500-300 mb thickness advection (gpm h^{-1})	-8.0 to +1.0	-4.0 to +4.0	-2.1	-1.4
500 mb vorticity advection (represented by number of height contour and vorticity isoline intersections)	-3 to +4	0 to +2	+1.0	+0.9
700 mb vertical velocity forecast (μb s^{-1})	-1 to +3	-1 to +1	+1.6	+0.6

environment. This difference is reflected by both the 850 mb mixing ratio and precipitable water. Second, the MCC low-level water vapor processes appear much more vigorous. Vapor advection is more than three times greater while vapor flux convergence is almost twice as great. The convergence value of .46 g $kg^{-1}h^{-1}$ compares fairly well with Maddox's (1981) prestorm value of 0.32 g kg^{-1} h^{-1}. A significant difference exists between the advection values, however. Maddox obtained a value of about -0.03 g kg^{-1} h^{-1} compared to the +0.20 g kg^{-1} h^{-1} obtained in this study. A significant part of this difference may be due to either sample size or differing evaluation techniques. Maddox determined the average value over an area larger than the storms IR satellite image. Maximum values occurring within the smaller radar echo region were used for this study. The final observation concerns thickness advection. Mean low-level warm advection is more than three times greater for the MCC cases. While upper-level cold advection is greater also, the difference is much smaller. Compared to earlier studies, the low-level warm advection value of +2.5 gpm h^{-1} is slightly low. Maddox (1983) reported an approximate value of +3.5 gpm h^{-1} in his investigation of ten MCCs. Hales (1982), in an investigation of seventeen tornado producing storms, reported an average value of +3.0 gpm h^{-1}.

b. <u>Statistical Comparison of Means</u>

Results from the statistical comparison of MCC to non-MCC mean values are shown in Table 9. For each variable, the α level is listed at which the two mean values are determined to be significantly

Table 9. Alpha (α) levels at which the corresponding MCC and non-MCC mean values were determined to be significantly different. Only levels between 0 and 0.5 were considered.

Parameter	Level
850 mb mixing ratio	.10
850 mb advection of water vapor	.05
850 mb flux divergence of water vapor	.40
Surface-to-500 mb average relative humidity	None
Precipitable water	.10
Totals Index	.20
Total Energy Index	.10
1000-700 mb thickness advection	.05
500-300 mb thickness advection	None
500 mb vorticity advection	None
700 mb vertical velocity forecast	.20

different. These α levels express the probability of erroneously concluding that the two values come from different populations. Therefore, those variables having large α levels should be of little value in distinguishing between MCC and non-MCC prestorm environments. Statistical results imply that surface-to-500 mb average relative humidity, 500-300 mb thickness advection, and vorticity advection are of no value. When initially comparing mean values, vapor flux convergence appeared promising as a distinguishing variable. The test for significant difference does not support this contention, however. The

large variability of vapor flux convergence makes it less effective. Vertical motion forecasts and the Totals Index show some value with an α level of .20. Of the two stability indices, however, the Total Energy Index appears more useful with an α level of .10. Other variables having an α level of .10 include the 850 mb mixing ratio and precipitable water. The two variables demonstrating the greatest potential for distinguishing between MCC and non-MCC environments are low-level thickness and low-level water vapor advection. Both were determined significant at the .05 level.

c.   Forecast Applications

The application of these results to the realm of forecasting should be viewed with caution due to the small sample size. Regardless, possible applications should be identified. In an attempt to distinguish between the MCC and non-MCC prestorm environments, scatter diagrams were used. Figure 7 illustrates one of these diagrams. For this diagram, low-level thickness advection is plotted against upper-level thickness advection for all eighteen storms. The nine MCCs are numbered and represented with circles. The nine non-MCCs are numbered also but represented with triangles. The storm numbers correspond to the numbers listed in Table 5. While the non-MCCs tend to cluster, the intermingling of several MCCs prevents a clear separation. This poor separation is not surprising, however, since upper-level thickness advection was determined to be an ineffective indicator for distinguishing between the two storm types.

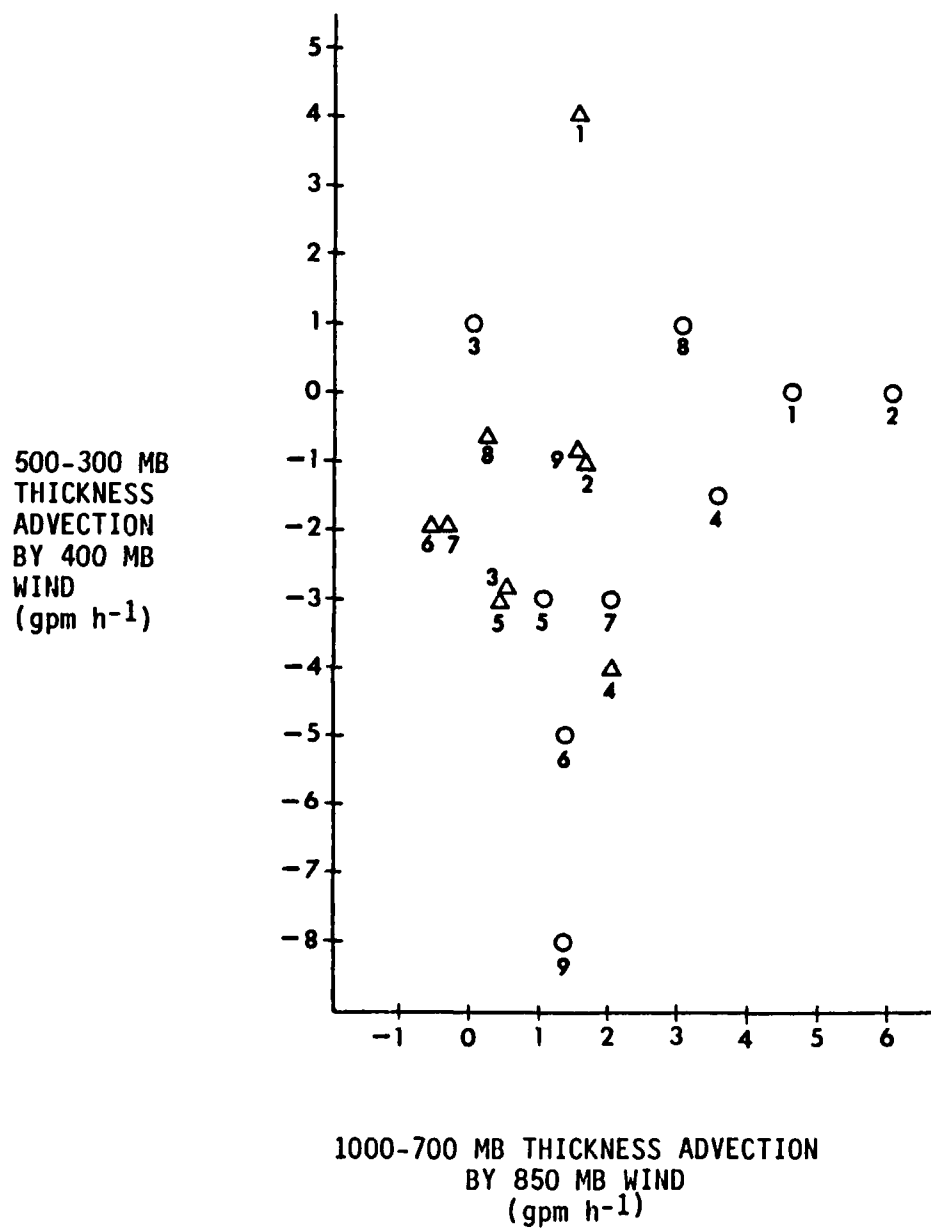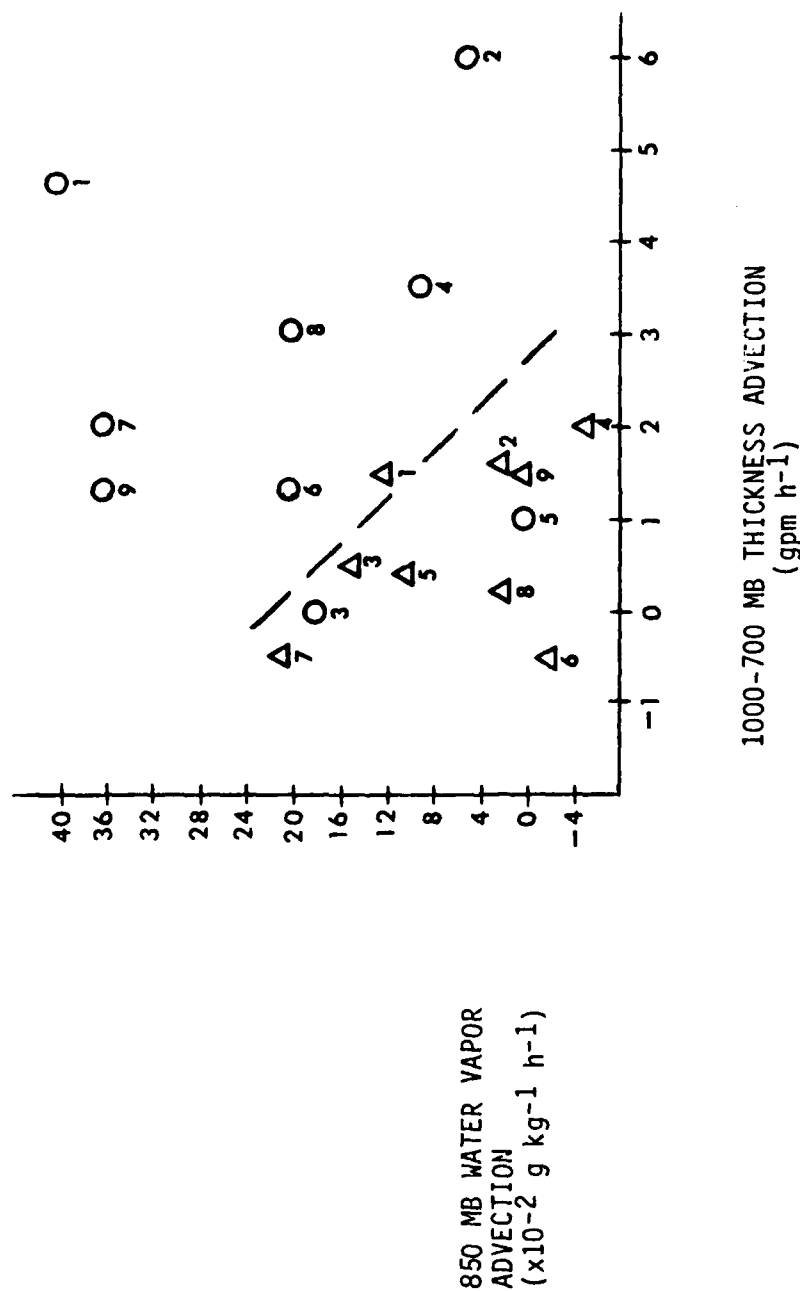Since low-level thickness advection and water vapor advection

Fig. 7. Scatter diagram plot of 1000-700 mb and 500-300 mb
thickness advection values for MCC (circles) and non-MCC (triangles)
storms. Storm numbers correspond to numbers in Table 5.

had the lowest α levels, a plot of these two variables should provide the best separation. This scatter diagram is depicted in Fig. 8 and does provide the best separation when compared to other possible combinations. With the exception of MCC numbers 3 and 5, a separation is evident.

In hopes of enhancing this separation, individual variables were combined in a physically realistic manner and replotted. This approach is best illustrated by returning to Fig. 7. Excluding MCC number 3, a relation between MCC low-level and upper-level advection was noted. Those MCCs characterized by strong low-level warm advection showed little advection aloft. However, those MCCs with weak low-level warm advection had significant compensating values of cold advection aloft. The non-MCCs did not demonstrate a similar relationship. Thus, a term including both low and upper-level advection might provide a better separation of storm types. This idea was tested in the following manner. A single term was formed by subtracting the 500-300 mb thickness advection value from the corresponding 1000-700 mb thickness advection value. Although equivalent rates of thickness advection within the two layers produce different rates of mean virtual temperature advection, the difference was not considered large enough to make weighting necessary. The resulting term, named the Differential Advection Index (DAI), provides a measure of the change in stability with time. Positive values indicate that the lapse rate is destabilizing with time; the larger the value, the greater the rate of change will be. After determining the DAI value for each storm, means were computed for the MCCs and non-MCCs. Applying the Student t test, the

Fig. 8. Scatter diagram plot of 1000-700 mb thickness advection and 850 mb water vapor advection for MCC (circles) and non-MCC (triangles) storms. Storm numbers correspond to numbers in Table 5. When used as a forecast nomogram, the area above the dashed line represents conditions favorable for MCC formation.

means were determined to be significantly different at the .10 α level. Thus, the combination process greatly increased the value of upper-level advection as a distinguishing factor. Figure 9 shows the storm separation achieved by plotting the 850 mb mixing ratio against the DAI. Compared to Fig. 8, this scatter diagram does a better job of separating MCC numbers 3 and 5 from the non-MCC storms. Non-MCC number 4, however, is now located in the midst of the MCC region. It is worth noting that number 4 was a large thunderstorm system that developed in the same region in which an MCC had occurred the previous day. The storm's environment possibly was still quite similar to that of the MCC.

Since low-level thickness and water vapor advection had provided fairly good separation when plotted against one another, an effort was made to combine these two variables. A clue to combining these two terms was provided by Darkow's development of the Total Energy Index. His index is based upon the difference in static energy at the 500 mb and 850 mb levels. The energy totals at each level are determined by calculating the contributions of sensible heat, latent heat, and potential energy. If potential energy is ignored, a method is thus available for combining the thickness and water vapor advection variables. Using advection, however, gives an estimate of the rate of change of energy rather than an actual energy total. This method is described in Appendix B. Thus, the energy rate of change at 850 mb was computed for each storm, averaged for the two storm types, and then tested for its ability to distinguish between MCC and non-MCC storm environments. The means were determined to be significantly
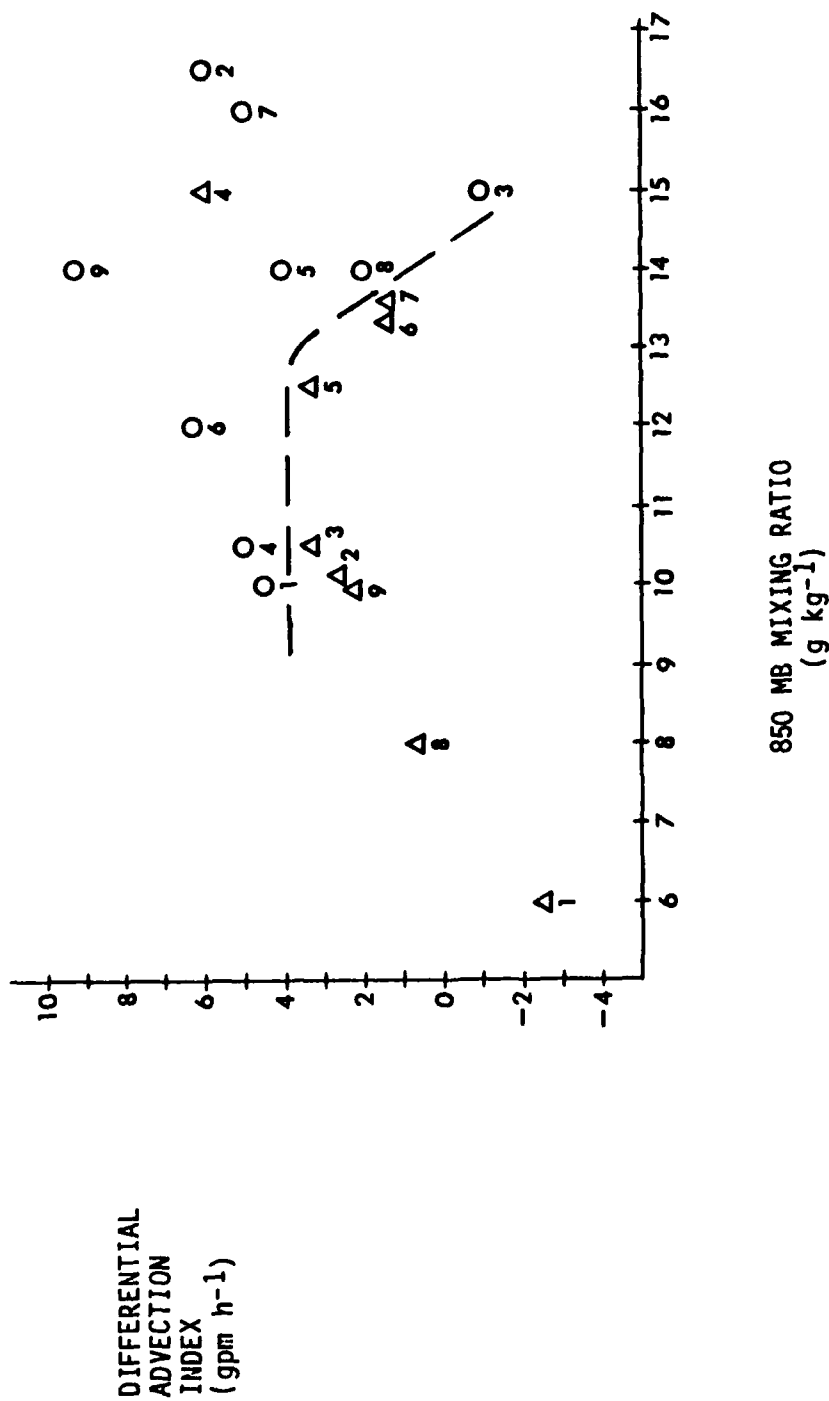
Fig. 9. Scatter diagram plot of 850 mb mixing ratio and Differential Advection Index for MCC (circles) and non-MCC (triangles) storms. Storm numbers correspond to numbers in Table 5. When used as a forecast nomogram, the area above the dashed line represents conditions favorable for MCC formations.

different at the .01 α level.

Additional scatter diagrams were drawn utilizing the 850 mb energy rate of change. Figure 10 shows the 850 mb mixing ratio plotted against the energy rate of change. While grouping is good, differences between MCC number 5 and non-MCC number 4 remain unresolved. Figure 11 shows a plot of the energy rate of change against the adjusted Total Energy Index. Using the energy rate of change values previously calculated for each storm, 850 mb static energy totals were computed for the time 0000 GMT +7 h. In turn, these 850 mb energy totals were used to compute an adjusted Total Energy Index value for each storm. The projected stability values were valid closer to the MCCs' formation times and, thus, hopefully more representative of the formation environment. Regardless, scatter diagram results remained essentially the same. Figure 12 depicts the final scatter diagram. The energy rate of change has been plotted against the DAI. Grouping is quite good but, again, complete separation is not attained. Table 10 provides a summary of the new variables derived. In addition, it depicts the corresponding MCC and non-MCC mean values and the α levels at which these mean values are determined to be significantly different.

Based upon the scatter diagram results, Figs. 8, 9, 10, and 12 are recommended for use as experimental MCC forecast nomograms. For each one, the region above the dashed line represents environmental conditions favorable for MCC development. No single nomogram incorporates all of the variables found useful in distinguishing between MCC and non-MCC prestorm environments. Each provides a different perspective. Therefore, probably all of the graphs should be used
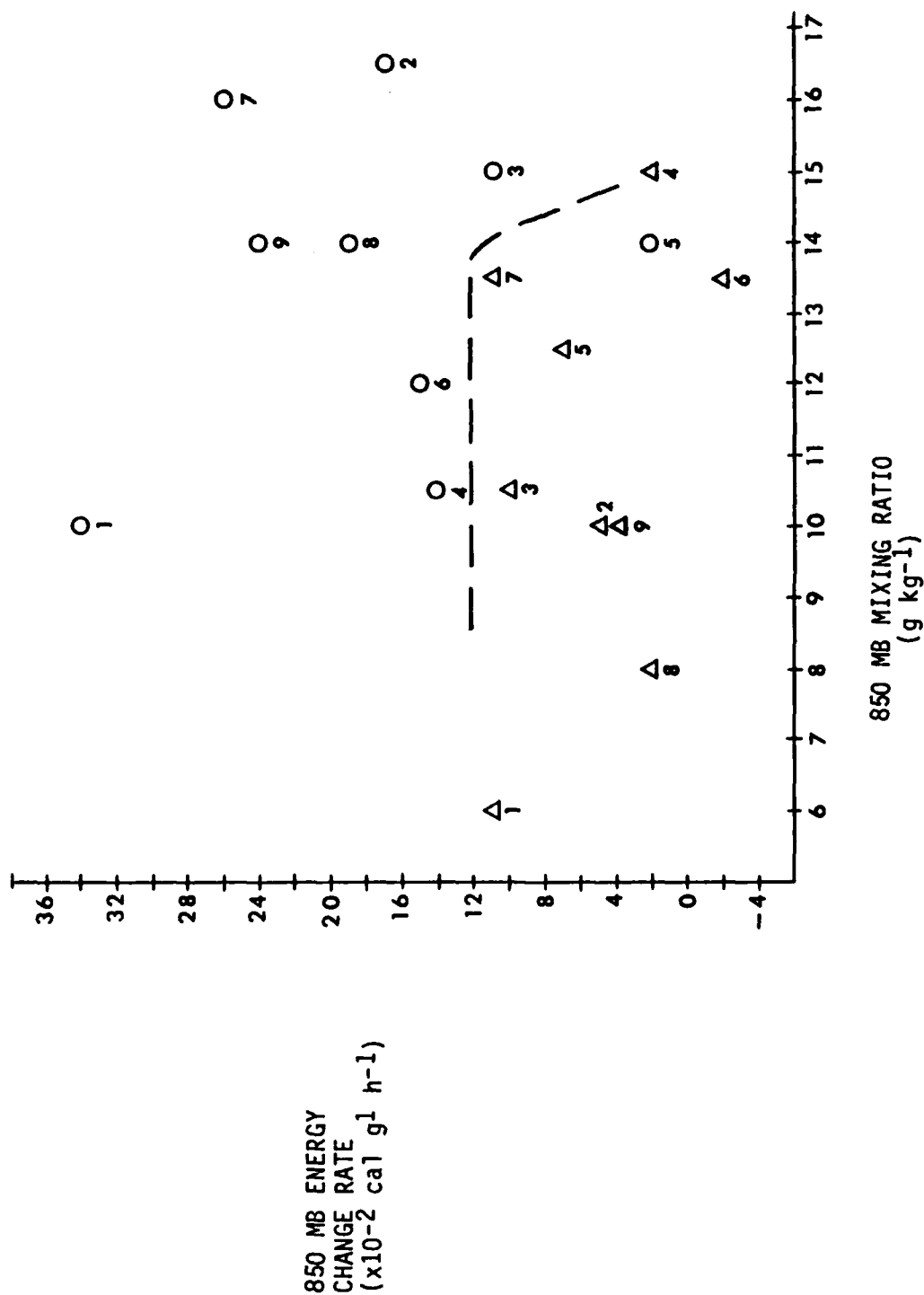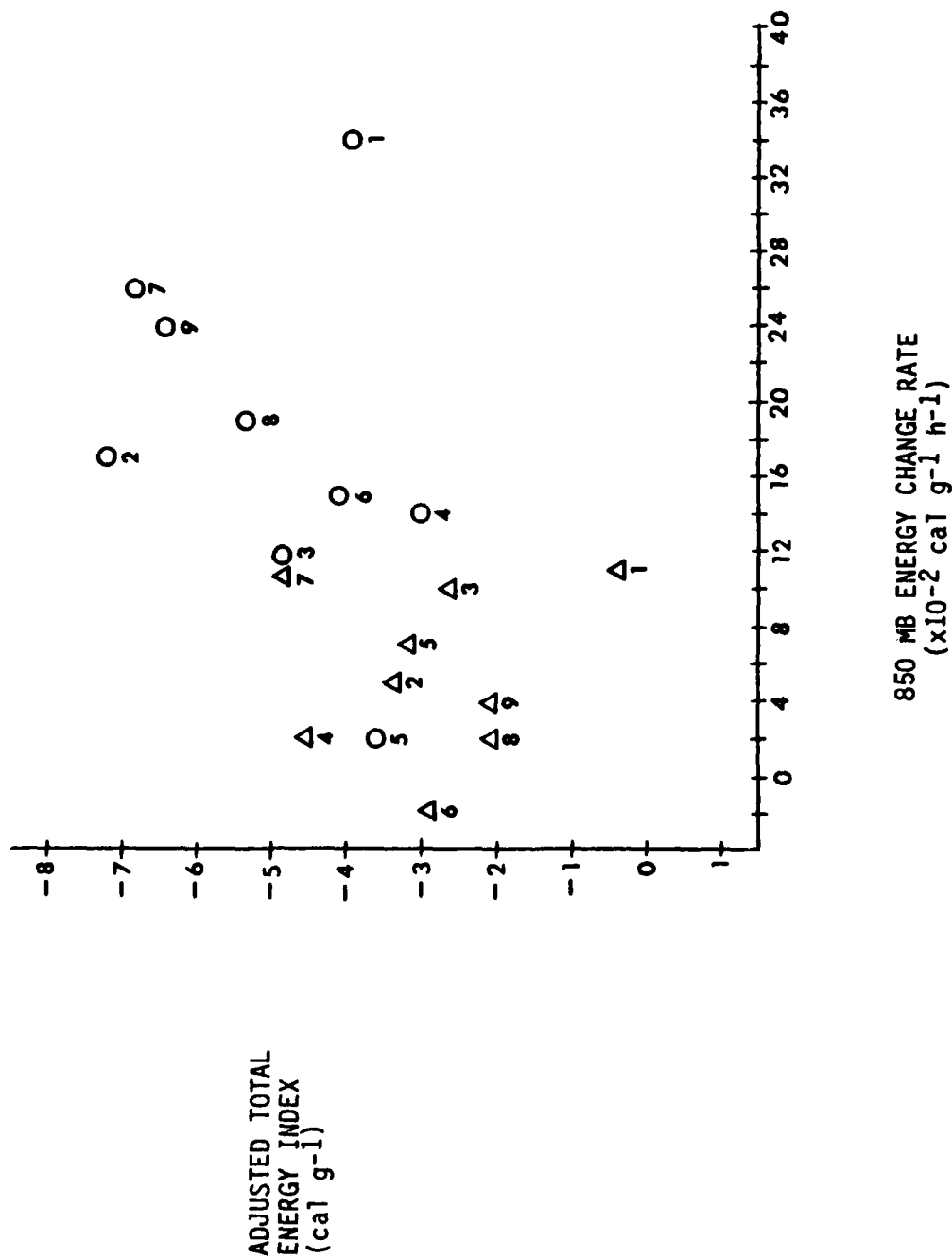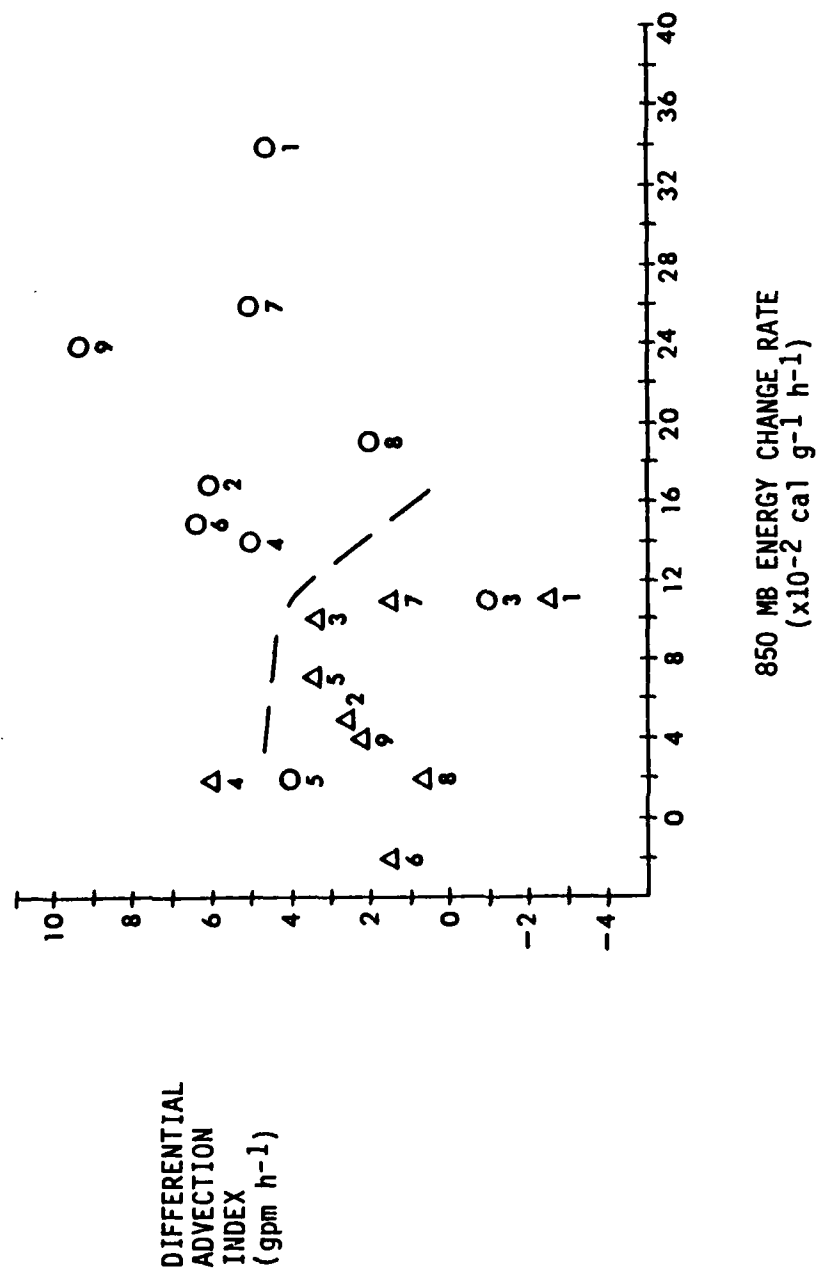
Fig. 10. Scatter diagram plot of 850 mb mixing ratio and 850 mb energy change rate for MCC (circles) and non-MCC (triangles) storms. Storm numbers correspond to numbers in Table 5. When used as a forecast nomogram, the area above the dashed line represents conditions favorable for MCC formations.

ADJUSTED TOTAL
ENERGY INDEX
(cal g⁻¹)

850 MB ENERGY CHANGE RATE
(x10⁻² cal g⁻¹ h⁻¹)

Fig. 11. Scatter diagram plot of 850 mb energy change rate and adjusted Total Energy Index
for MCC (circles) and non-MCC (triangles) storms. Storm numbers correspond to numbers in Table 5.

Fig. 12. Scatter diagram plot of 850 mb energy change rate and Differential Advection Index for MCC (circles) and non-MCC (triangles) storms. Storm numbers correspond to numbers in Table 5. When used as a forecast nomogram, the area above the dashed line represents conditions favorable for MCC formation.

Table 10. The new variables formed, their mean MCC and non-MCC values, and the alpha (α) level at which each pair was determined to be statistically different.

PARAMETER	MEAN VALUE		
	MCC	NON-MCC	α LEVEL
Differential Advection Index (gpm h^{-1})	4.6	2.1	.10
850 mb Energy Rate of Change (cal g^{-1} h^{-1})	.18	.05	.01
Adjusted Total Energy Index (cal g^{-1})	-5.0	-2.9	.01

when evaluating MCC formation potential; this procedure is especially important for borderline storm environments. These graphs should be used for only short term forecasts since they assume adiabatic conditions and perfect advection.

7.   CONCLUSIONS

Statistical results suggest that certain atmospheric meteorological variables can be used to distinguish bctween MCC and non-MCC prestorm environments. Variables of statistical value include the 850 mb mixing ratio, 850 mb water vapor advection, precipitable water, the Total Energy Index, and 1000-700 mb thickness advection. The MCC and non-MCC mean values for each of these variables were determined to be significantly different at n α level of .10 or less.

The scatter diagram plots reinforce the statistical findings. Of the eleven original variables, low-level thickness advection and low-level water vapor advection provide the best graphical separation of MCC and non-MCC storms. New indicators developed by combining variables also show skill in graphically separating the two storm types. While upper-level advection by itself is a poor indicator, its combination with low-level advection provides a more complete measure of differential advection and, thus, is more useful. Low-level thickness and water vapor advection have been combined to provide an estimate of the energy change rate at 850 mb. Of all the variables investigated, this energy rate of change term provides the best distinction between MCC and non-MCC prestorm environments. This result implies that abnormally large energy increases within the low-levels are required for MCC development.

MCC and non-MCC storm separation is apparent on the scatter diagrams. While complete separation is never attained, the results are encouraging, especially considering the difficulty of the task. One cannot expect synoptic data to provide a perfect distinction

between the environments of two mesoscale events so similar in nature.

While investigative results are encouraging, they cannot be accepted with a large degree of confidence. In general, differences between the MCC and non-MCC mean values are only slightly larger than the associated RMS errors. Furthermore, the small number of cases examined reduces the reliability of the statistical test applied. A final consideration concerns storm location. Seven of the nine MCCs studied formed in either eastern Kansas or Missouri. Thus, mean values obtained for the MCCs may have limited application elsewhere, especially for the drier western plains region.

Additional investigations considering a larger number of storms are needed to verify the results obtained here. A greater number of case studies would allow a more reliable statistical analysis. If results continue to be encouraging, a sound basis will exist for the development of operational forecast procedures and techniques. While synoptic data do not provide sufficient information to pinpoint the location and timing of severe weather events, they have proven useful in identifying those areas most susceptible to such weather. Use of synoptic data to identify those environments favorable for MCC development appears feasible. Such guidance could have a significant impact upon regional forecast preparation, especially when considering the potential for heavy rains, flooding, hail and tornadoes.

REFERENCES

Barnes, S.L., 1964: A technique for maximizing details in numerical weather map analysis. J. Appl. Meteor., 3, 396-409.

Cotton, W. R., R. L. George, P. J. Wetzel and R. L. McAnelly, 1983: A long-lived mesoscale convective complex. Part I: The mountain-generated component. Mon. Wea. Rev., 111, 1893-1918.

Crawford, M. E., 1950: A synoptic study of instability lines. Bull. Amer. Meteor. Soc., 31, 349-357.

Darkow, G. L., 1968: The total energy environment of severe storms. J. Appl. Meteor., 7, 199-205.

Fritsch, J. M., R. A. Maddox and A. G. Barnston, 1981: The character of mesoscale convective complex precipitation and its contribution to warm season rainfall in the U.S. Preprints, Fourth Conf. on Hydrometeorology, Reno, Amer. Meteor. Soc., 94-99.

Fuelberg, H. E., 1974: Reduction and error analysis of the AVE II pilot experiment data. Nasa Contractor Report CR-120496. Marshall Space Flight Center, Alabama, 140 pp.

Fulks, J. R., 1951: The instability line. Compendium of Meteorology, Boston, Amer. Meteor. Soc., 647-654.

Hales, J. E., Jr., 1979: On the relationship of 250 mb positive vorticity advection and horizontal divergence to tornado and severe thunderstorm development. Preprints, 11th Conf. on Severe Local Storms, Kansas City, Amer. Meteor. Soc., 28-31.

_____, 1982: Relationship of selected synoptic scale parameters to significant tornado occurrences in 1980. Preprints, 12th Conf. on Severe Local Storms, San Antonio, Amer. Meteor. Soc., 139-142.

Holton, J.R., 1972: An Introduction to Dynamic Meteorology. Academic Press, New York, 319 pp.

MacDonald, J. D., 1952: On the formation of squall lines. Bull. Amer. Meteor. Soc., 33, 237-239.

Maddox, R. A., 1981: The structure and life-cycle of midlatitude mesoscale convective complexes. Atmos. Sci. Pap. No. 336, Dept. Atmos. Sci., Colorado State University, Fort Collins, 311 pp.

_____, 1983: Large-scale meteorological conditions associated with midlatitude mesoscale convective complexes. Mon. Wea. Rev., 111, 1475-1493.

_____, and C. A. Doswell, III, 1982: An examination of jet stream configurations, 500 mb vorticity advection and low-level thermal advection patterns during extended periods of intense convection. Mon. Wea. Rev., 110, 184-197.

_____, D. J. Perkey and J. M. Fritsch, 1981: Evolution of upper-tropospheric features during the development of a mesoscale convective complex. J. Atmos. Sci., 38, 1664-1674.

_____, D. M. Rogers and K. W. Howard, 1982: Mesoscale convective complexes over the United States during 1981 - annual summary. Mon. Wea. Rev., 110, 1501-1514.

_____, _____, _____, B. Heckman, N. Johnston and M. Mathews, 1983: An experiment in forecasting mesoscale convective weather systems. Manuscript prepared for Amer. Meteor. Soc. 13th Conf. on Severe Local Storms, October 1983, Tulsa, 13 pp.

Miller, R. C., 1967: Notes on analysis and severe storm forecasting procedures of the Military Weather Warning Center. AWS Tech. Rep. 200, Headquarters Air Weather Service, Scott AFB, 94 pp.

Palmen, E., and C. W. Newton, 1969: Atmospheric Circulation Systems, Their Structure ar Physical Interpretation. Academic Press, New York, 603 pp.

Rhea, J. O., 1966: A study of thunderstorm formation along dry lines. J. Appl. Meteor., 5, 58-63.

Rogers, D. M., and K. W. Howard, 1983: Mesoscale convective complexes over the United States during 1982. Mon. Wea. Rev., 111, 2363-2369.

Sienkiewicz, M. E., 1981: The moisture budget accompanying convective activity. Dept. Meteor., Texas A M University, College Station, 86 pp.

Wetzel, P. J., W. R. Cotton and R. L. McAnelly, 1982: The dynamic structure of the mesoscale convective complex - some case studies. Preprints, 12th Conf. on Severe Local Storms, San Antonio, Amer. Meteor. Soc., 265-268.

_____, _____, and _____, 1983: A long-lived mesoscale convective complex. Part II: Evolution and structure of the mature complex. Mon. Wea. Rev., 111, 1919-1937.

APPENDIX A

CHARTS FOR THE 15 AUGUST 1982 MCC

AND 9 AUGUST 1978 NON-MCC

Grid values of the first nine variables listed in Table 2 were computed for each MCC and non-MCC case; isopleths were then drawn by hand. NMC 500 mb Height/Vorticity Analysis and LFM vertical velocity forecast panels were used to represent the two final variables. Samples of these charts and NMC preducts are contained in this appendix. Figures A-1a through A-1k illustrate the fields associated with the 15 August 1982 MCC. Figures A-2a through A-2k illustrate the fields associated with the 9 August 1978 non-MCC.
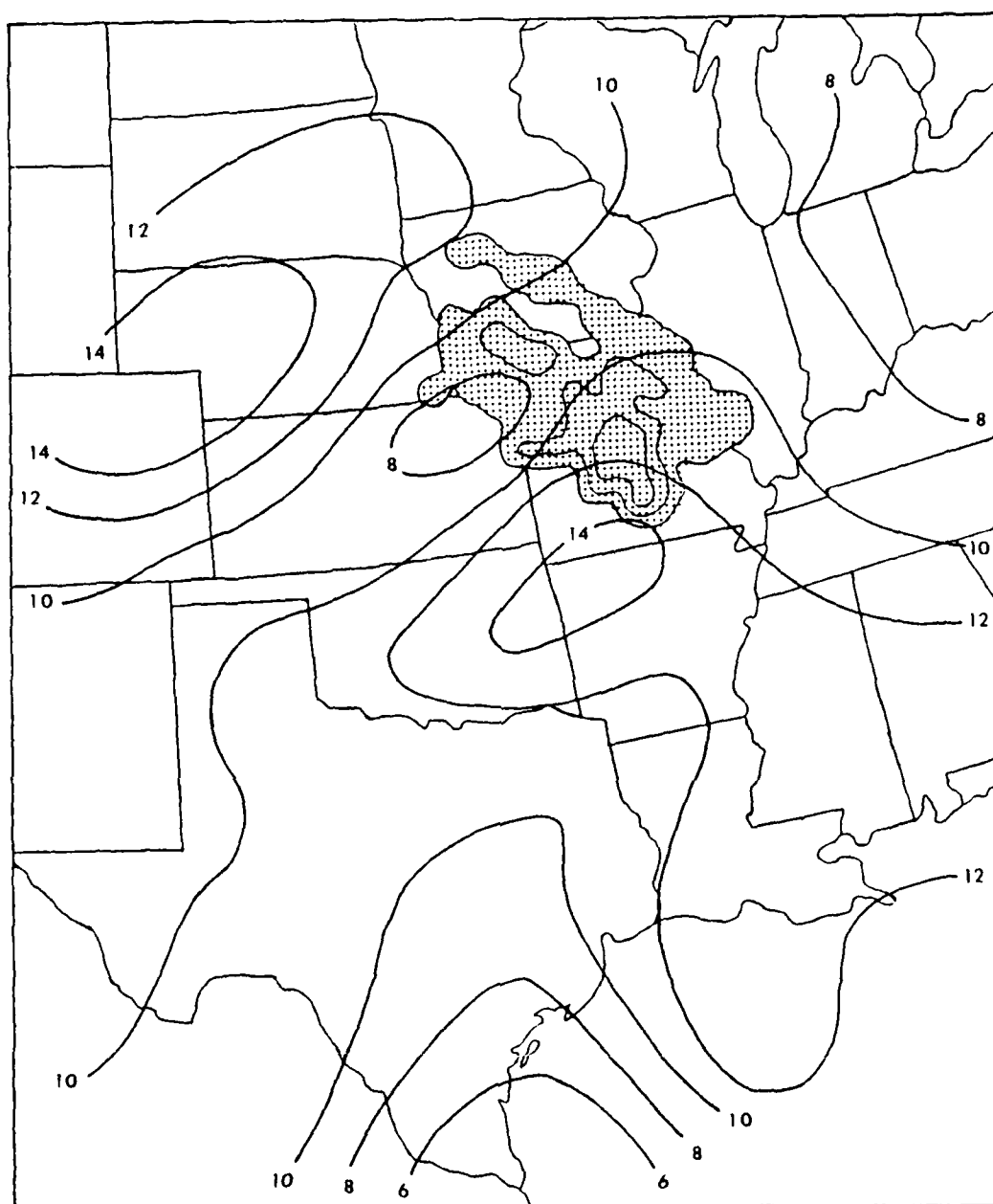
Fig. A-1a. 850 mb mixing ratio (g kg^{-1}) for 0000 GMT 15
August 1982. Stippled region depicts the MCC radar echo at 0835 GMT.
Radar echoes not a part of the MCC are not shown.
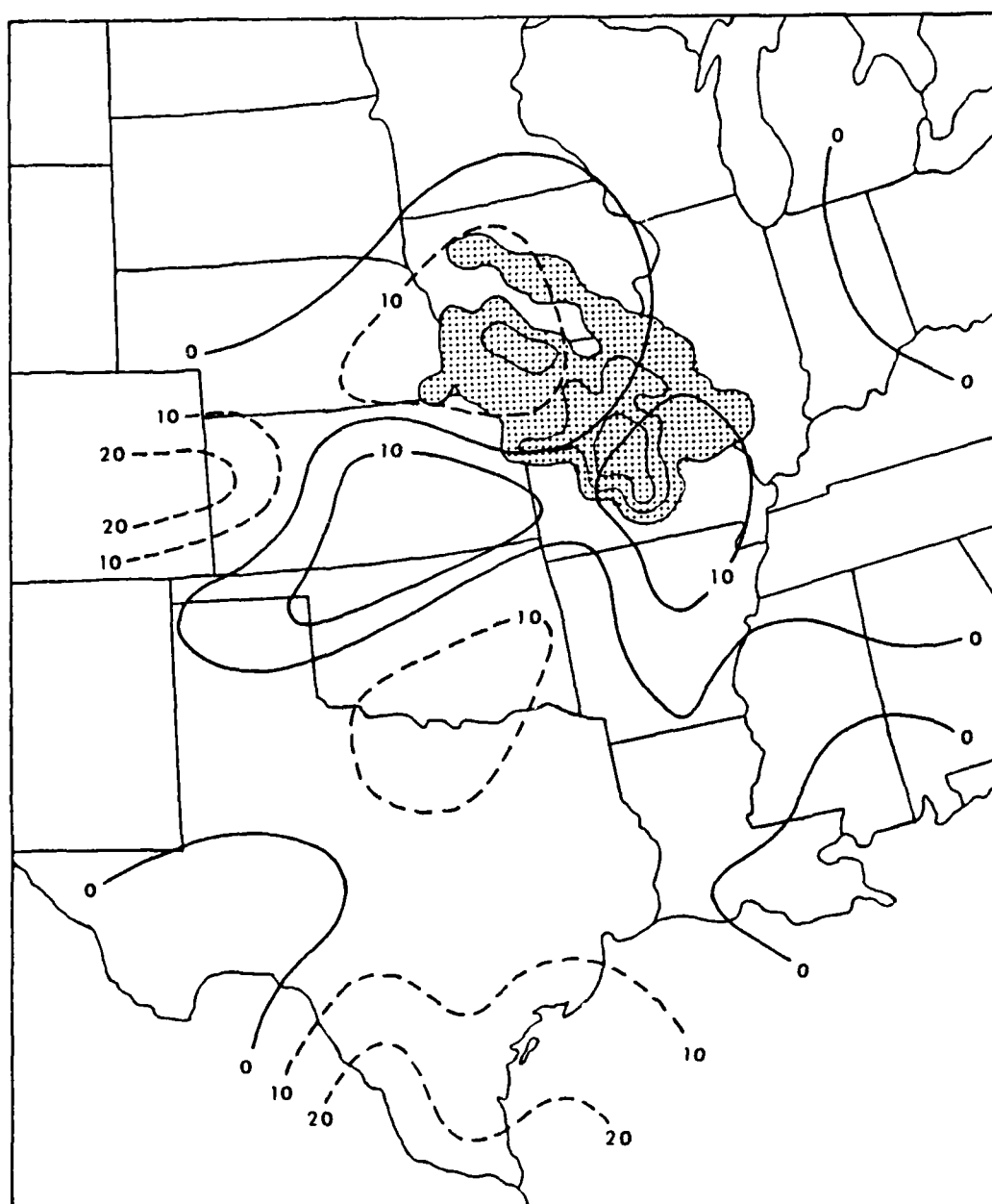
Fig. A-1b.   850 mb water vapor advection ($\times 10^{-2}$ g kg^{-1} h^{-1}) for 0000 GMT 15 August 1982.   Solid lines are positive and dashed lines are negative.   Stippled region depicts the MCC radar echo at 0835 GMT.
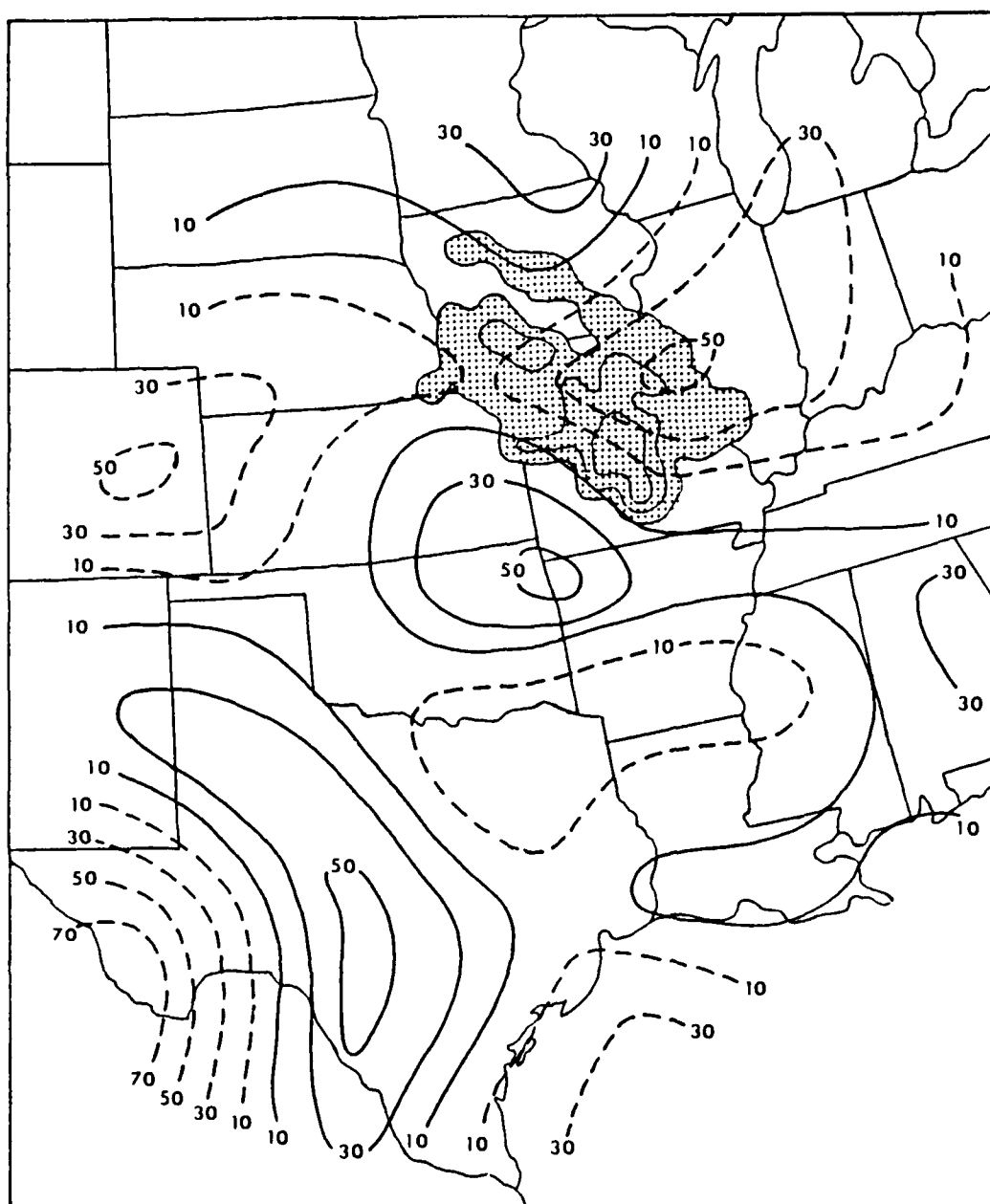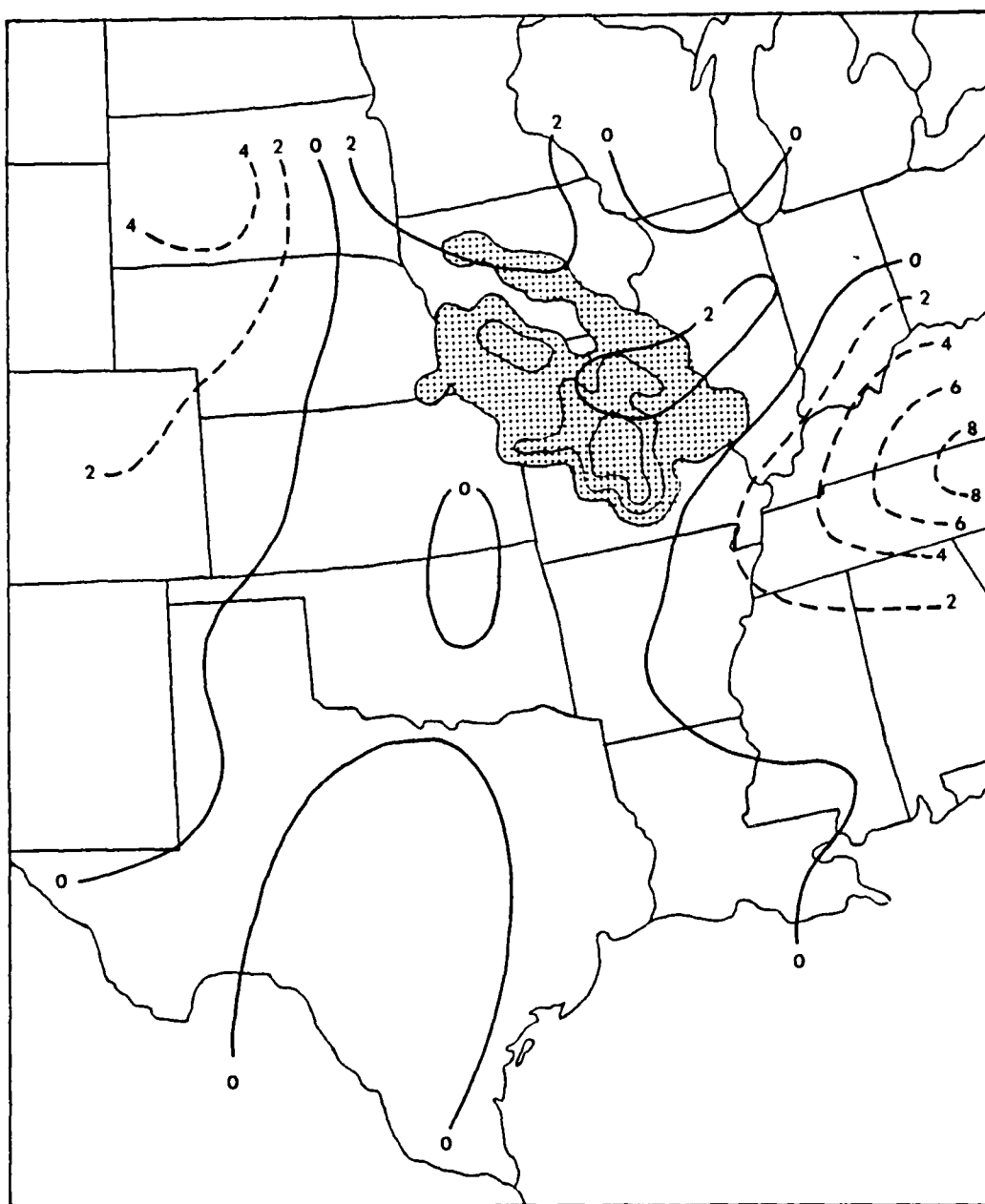
Fig. A-1c. 850 mb flux divergence of water vapor (x10^{-2} g kg^{-1} h^{-1}) for 0000 GMT 15 August 1982. Solid lines are positive and dashed lines are negative. Stippled region depicts the MCC radar echo at 0835 GMT.
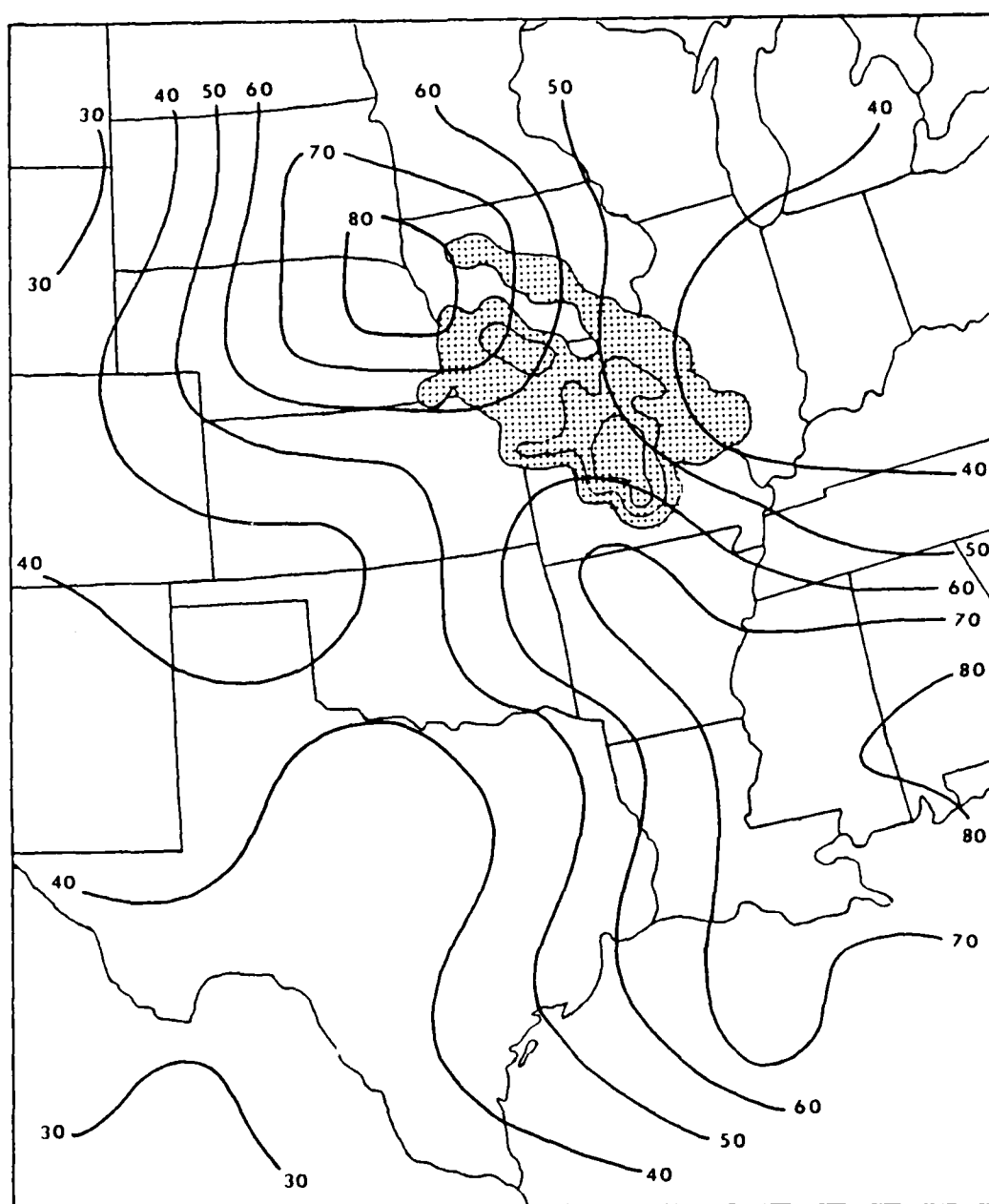
Fig. A-1d. Surface-to-500 mb average relative humidity (%) for 0000 GMT 15 August 1982. Stippled region depicts the MCC radar echo at 0835 GMT.
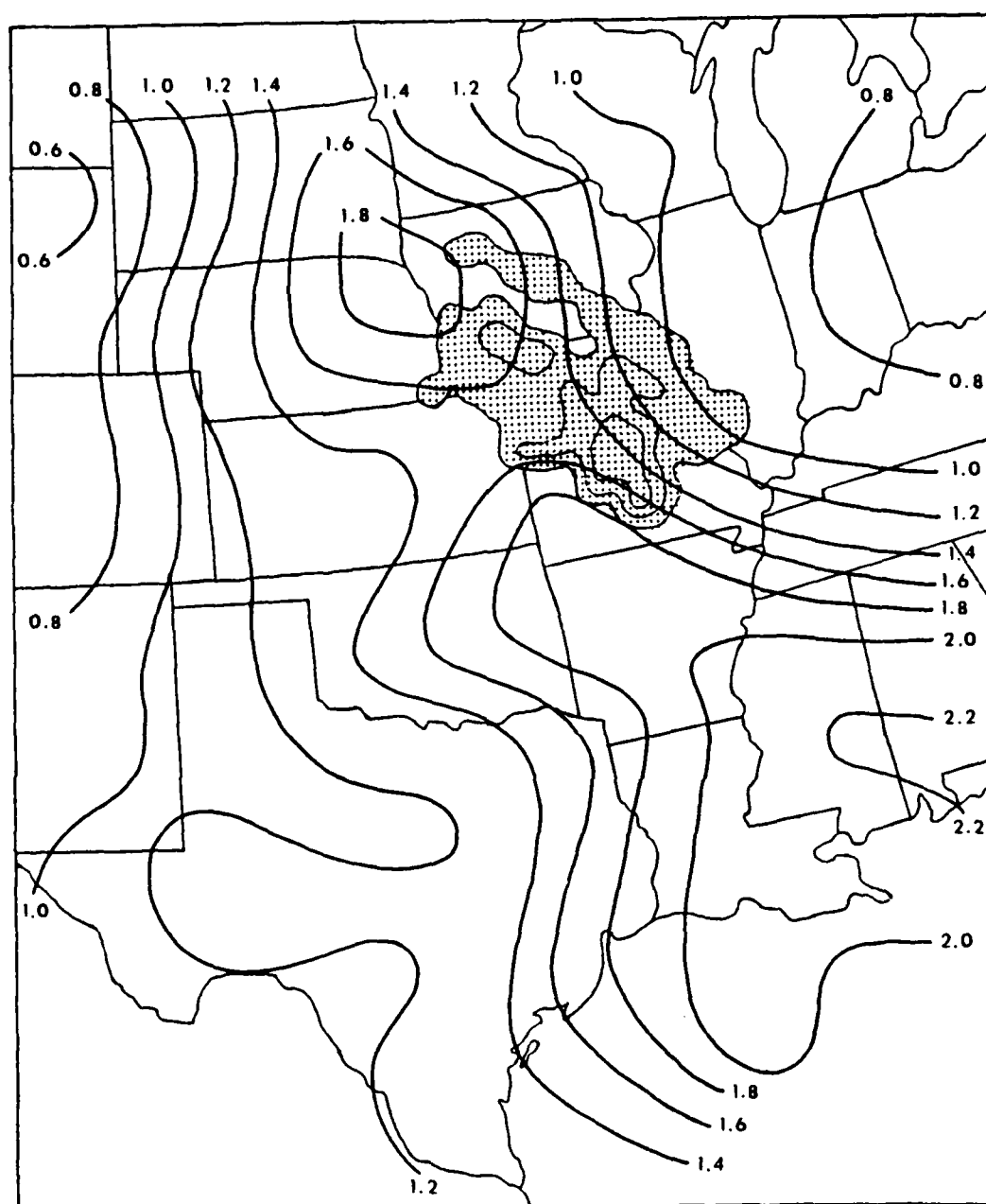
Fig. A-1e. Precipitable water (inches) for 0000 GMT 15 August 1982. Stippled region depicts the MCC radar echo at 0835 GMT.
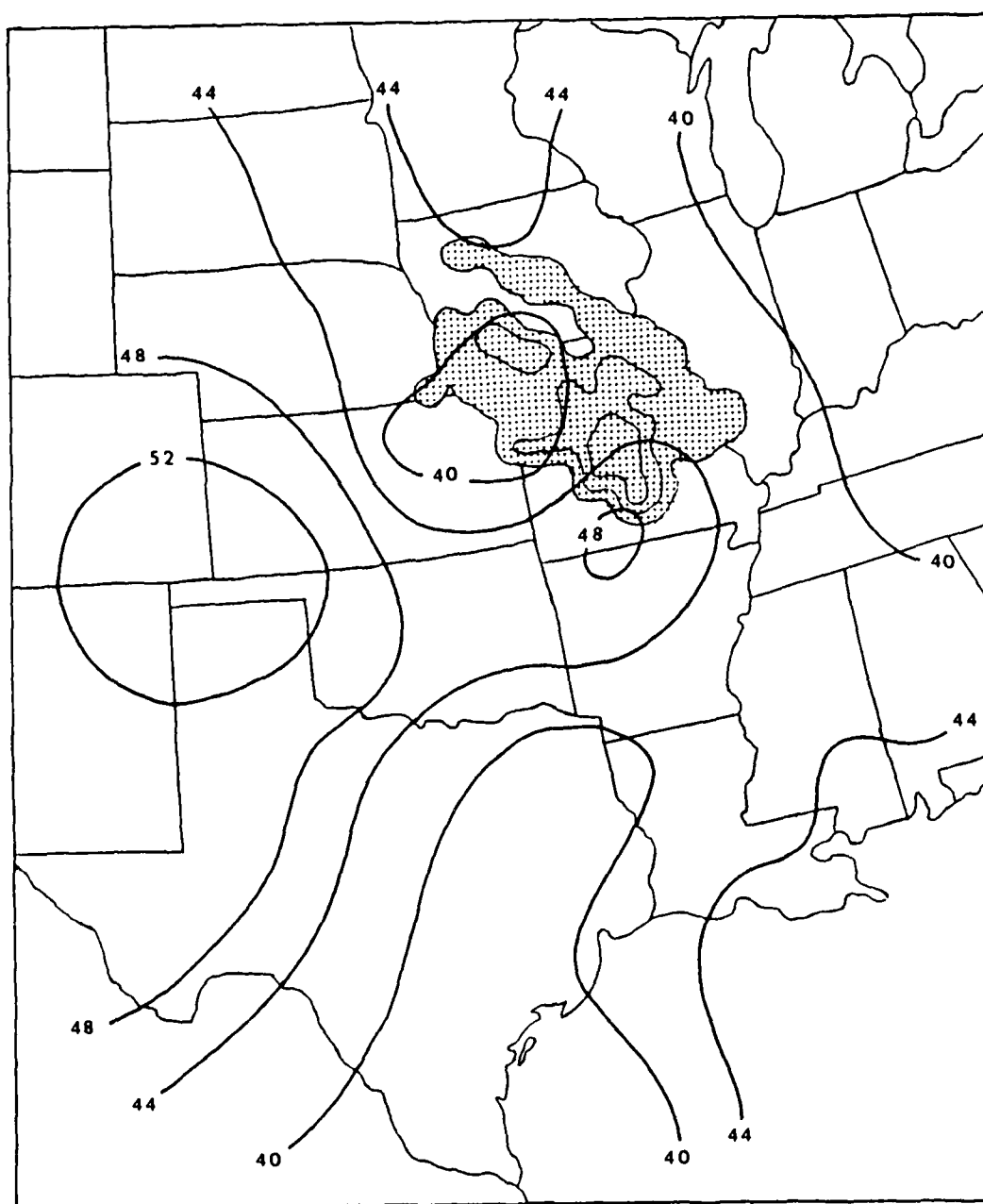
Fig. A-1f. Totals Index for 0000 GMT 15 August 1982. Stippled region depicts the MCC radar echo at 0835 GMT.
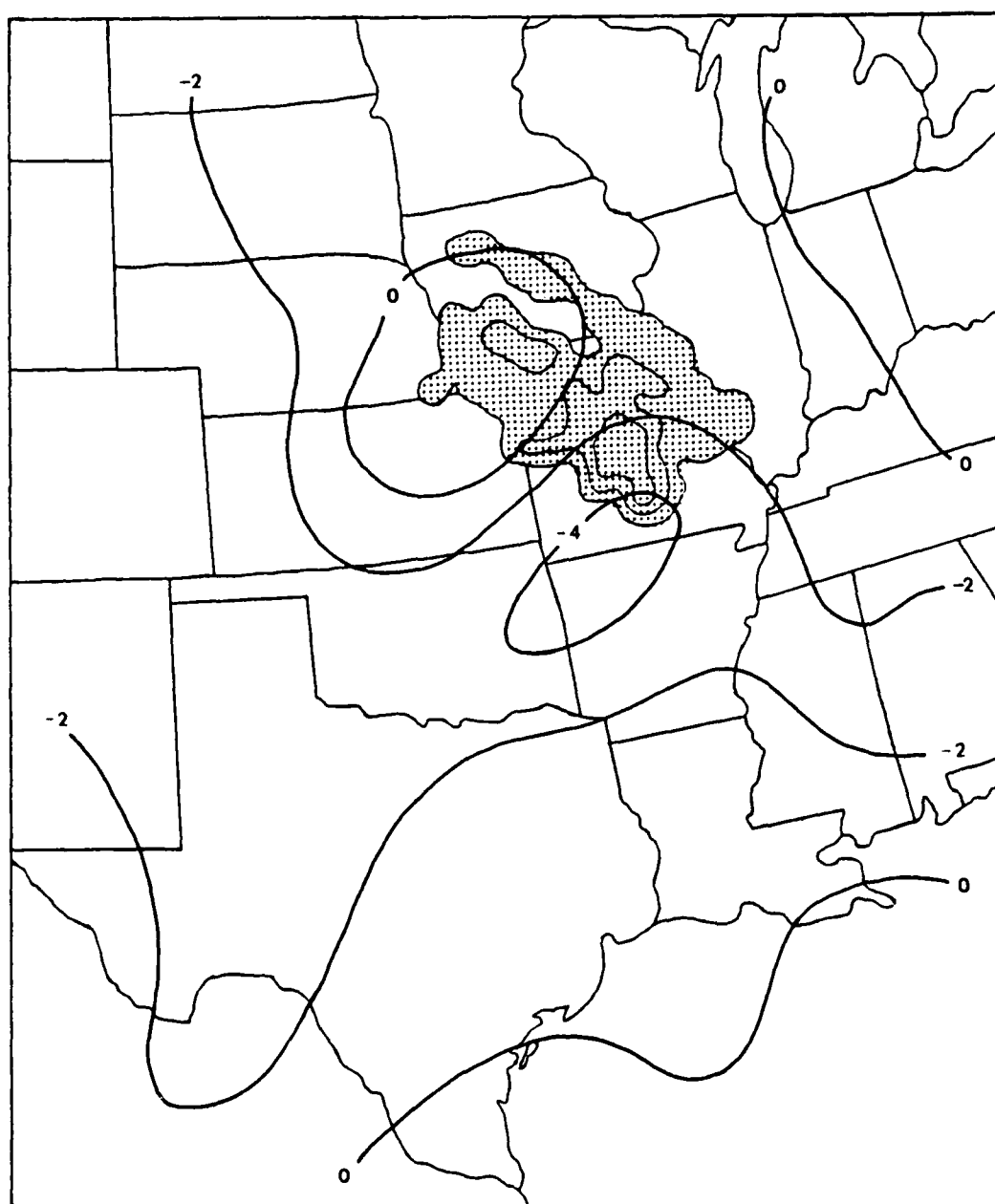
Fig. A-1g. Total Energy Index (cal g^{-1}) for 0000 GMT 15 August 1982. Stippled region depicts the MCC radar echo at 0835 GMT.
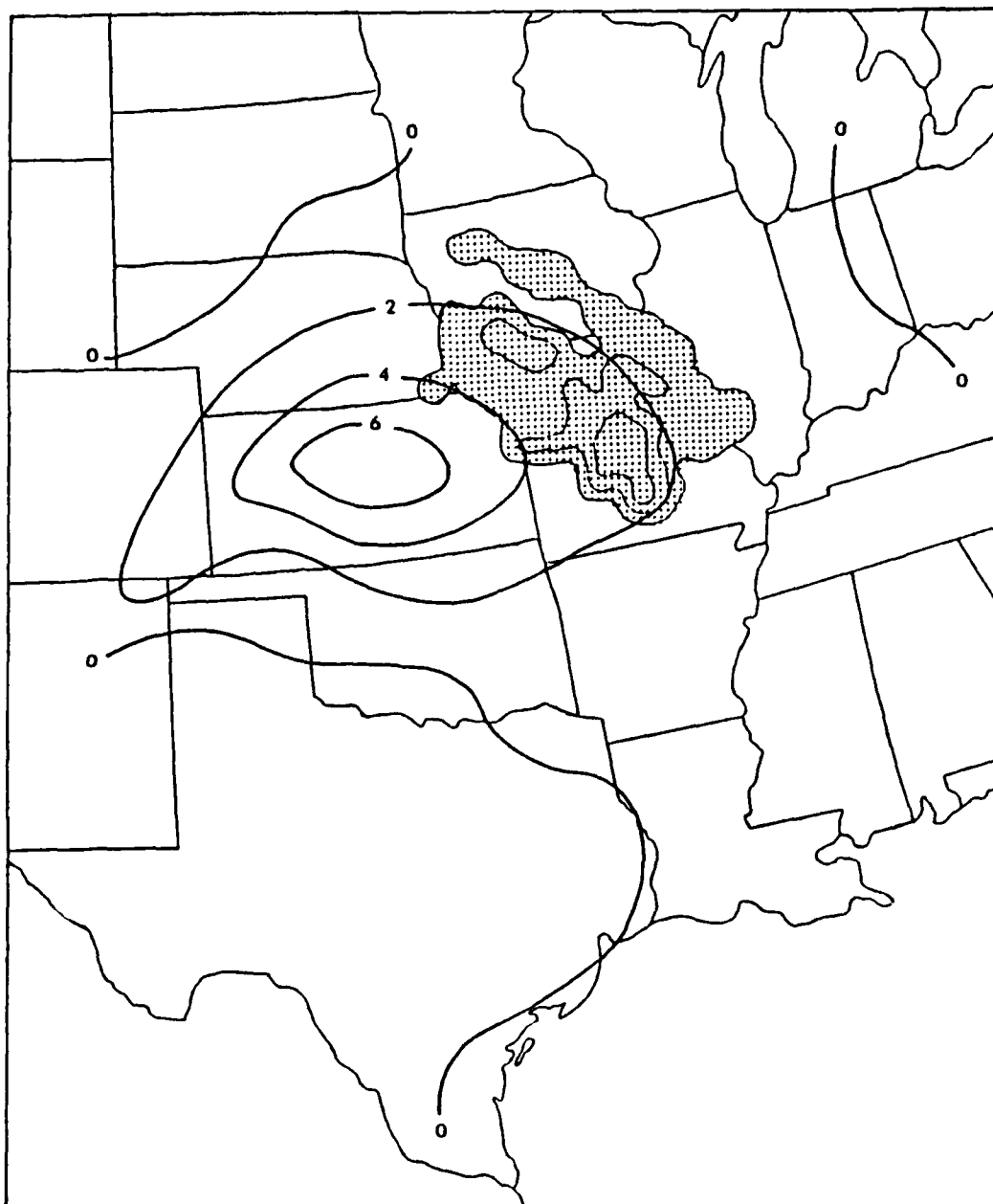
Fig. A-1h.   1000-700 mb thickness advection (gpm h^{-1}) by 850 mb wind for 0000 GMT 15 August 1982.   Solid lines are positive and dashed lines are negative.   Stippled region depicts the MCC radar echo at 0835 GMT.

Fig. A-1i. 500-300 mb thickness advection (gpm h^{-1}) by 400 mb wind for 0000 GMT 15 August 1982. Solid lines are positive and dashed lines are negative. Stippled region depicts the MCC radar echo at 0835 GMT.
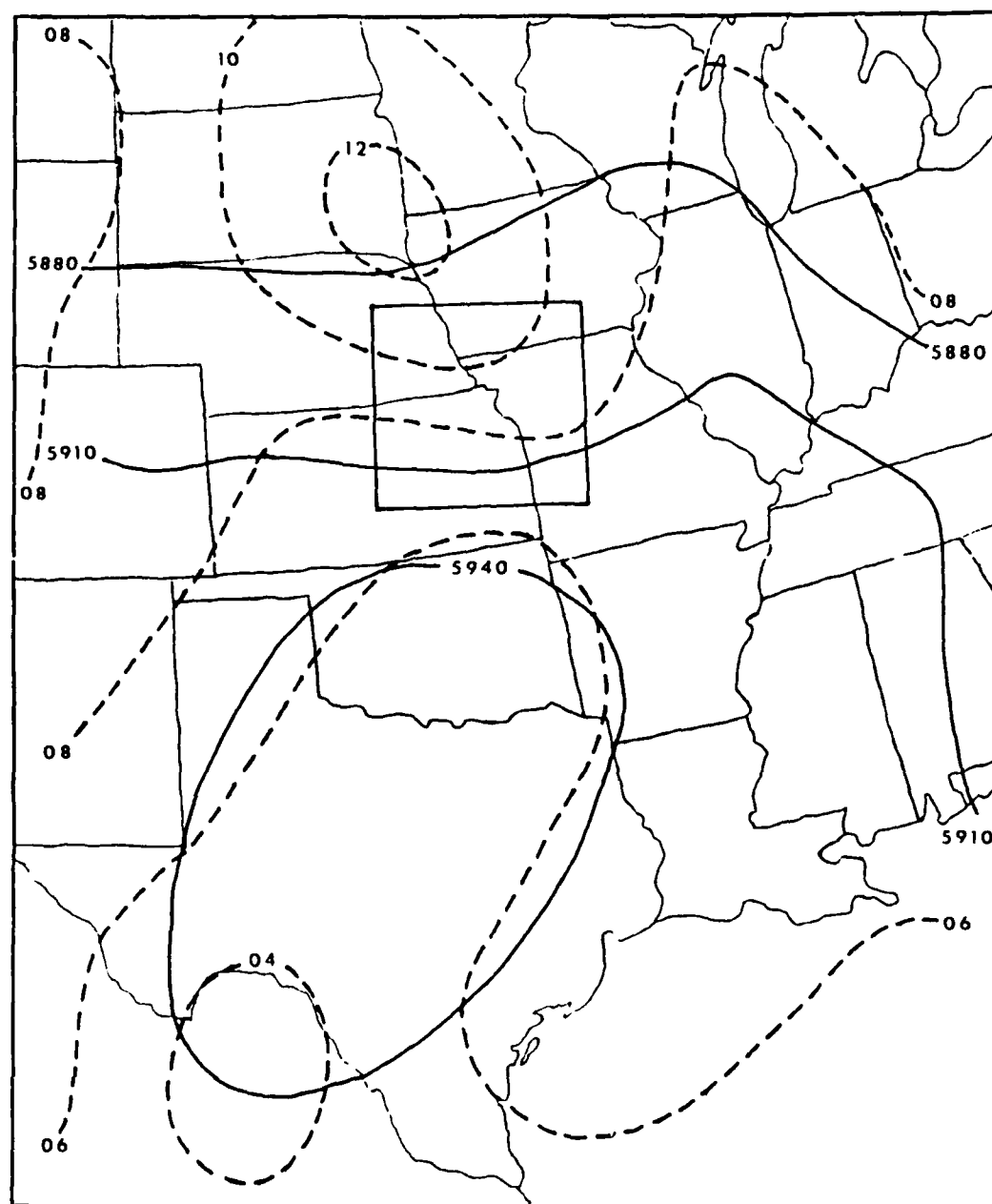
Fig. A-1j. NMC 500 mb Height/Vorticity Analysis Chart for 0000 GMT 15 August 1982. Units are gpm for height (solid lines) and ($\times 10^{-5}$ s^{-1}) for vorticity (dashed lines). The height/vorticity field within the box was used to estimate the type and intensity of vorticity advection into the MCC region.
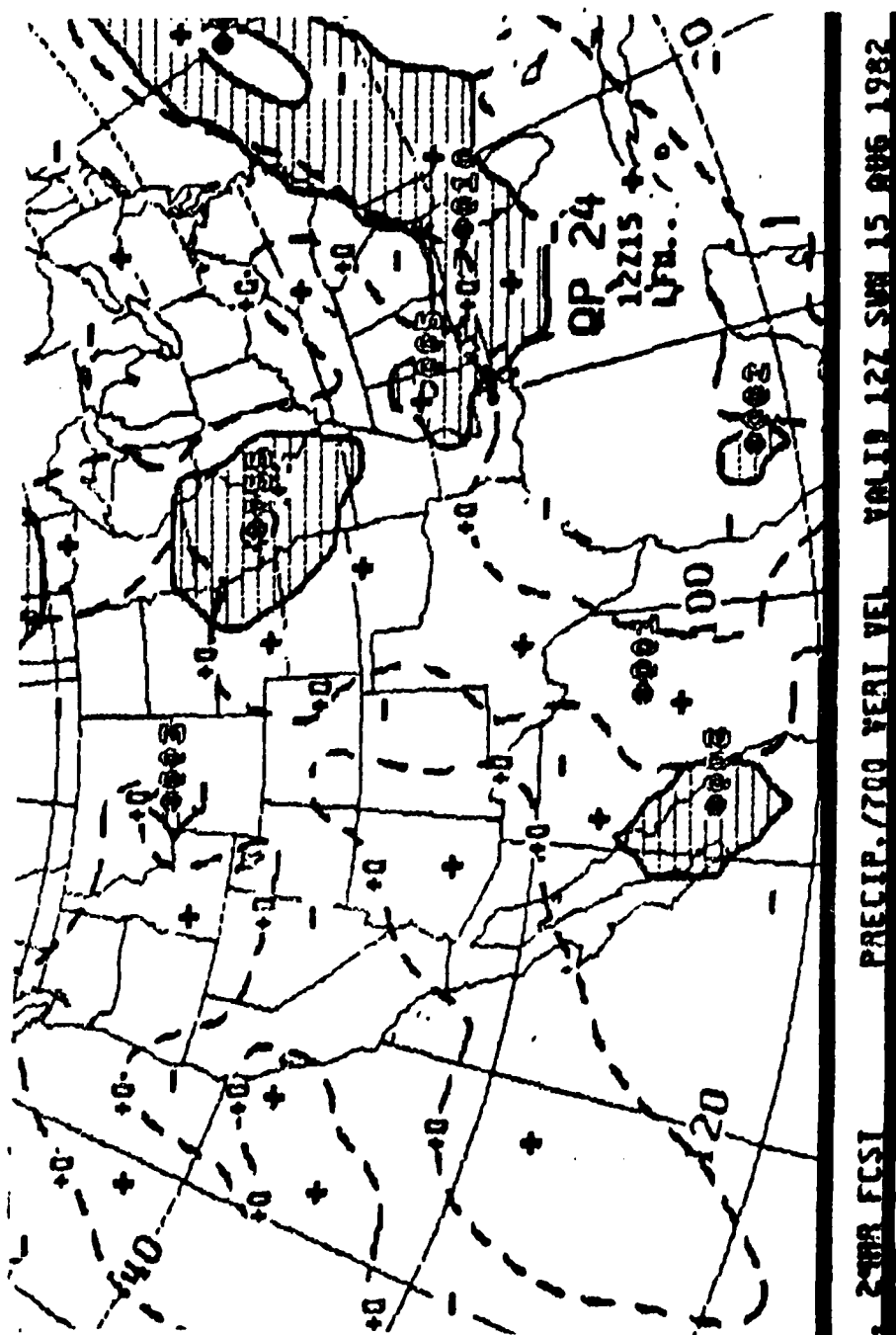
Fig. A-1k. LFM vertical velocity ($\mu b\ s^{-1}$) forecast chart for 1200 GMT 15 August 1982. Iso-lines of vertical velocity are dashed.
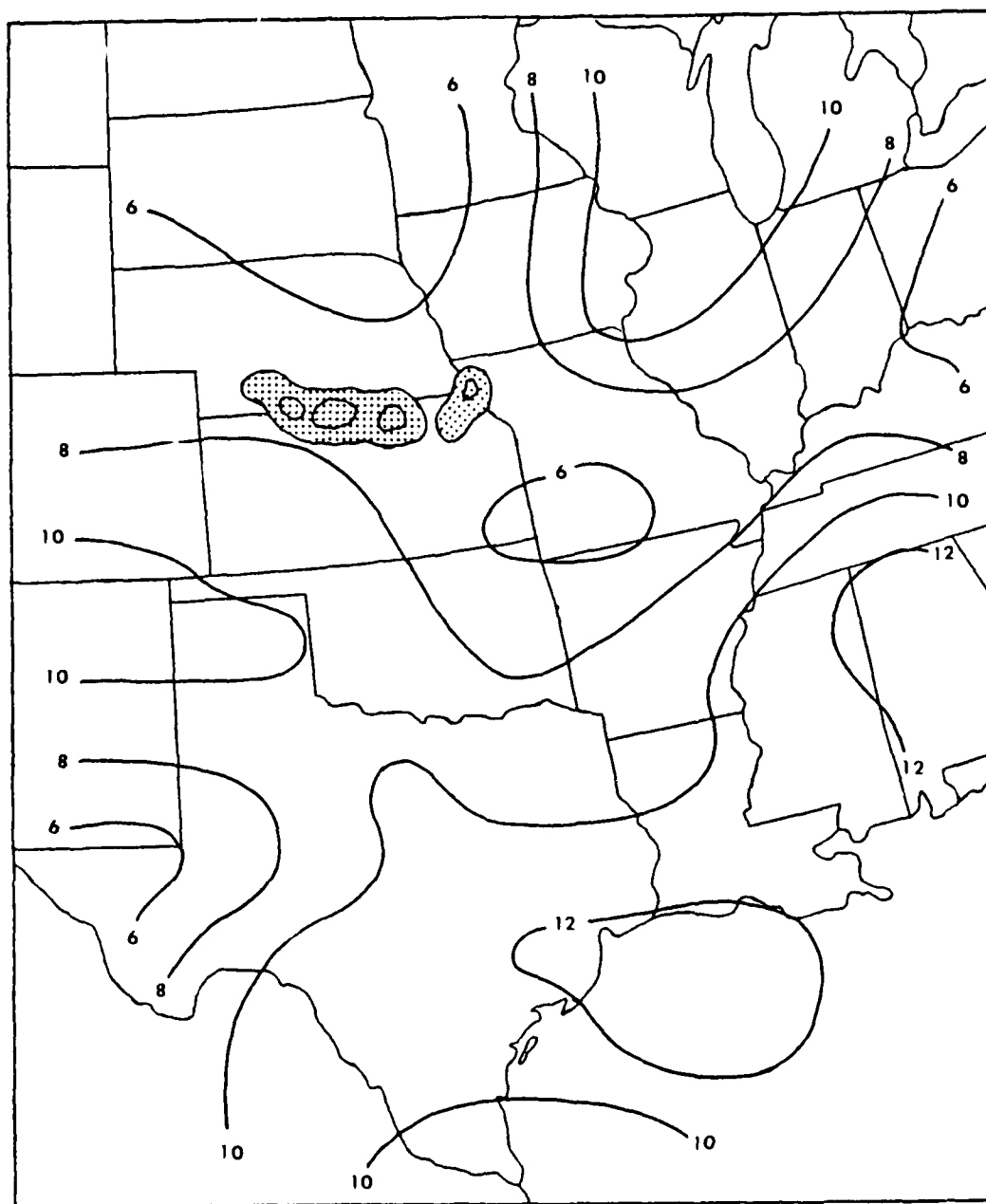
Fig. A-2a. 850 mb mixing ratio (g kg^{-1}) for 0000 GMT 9 August 1978. Stippled region depicts the non-MCC radar echo at 0435 GMT. Radar echoes not a part of this storm system are not shown.
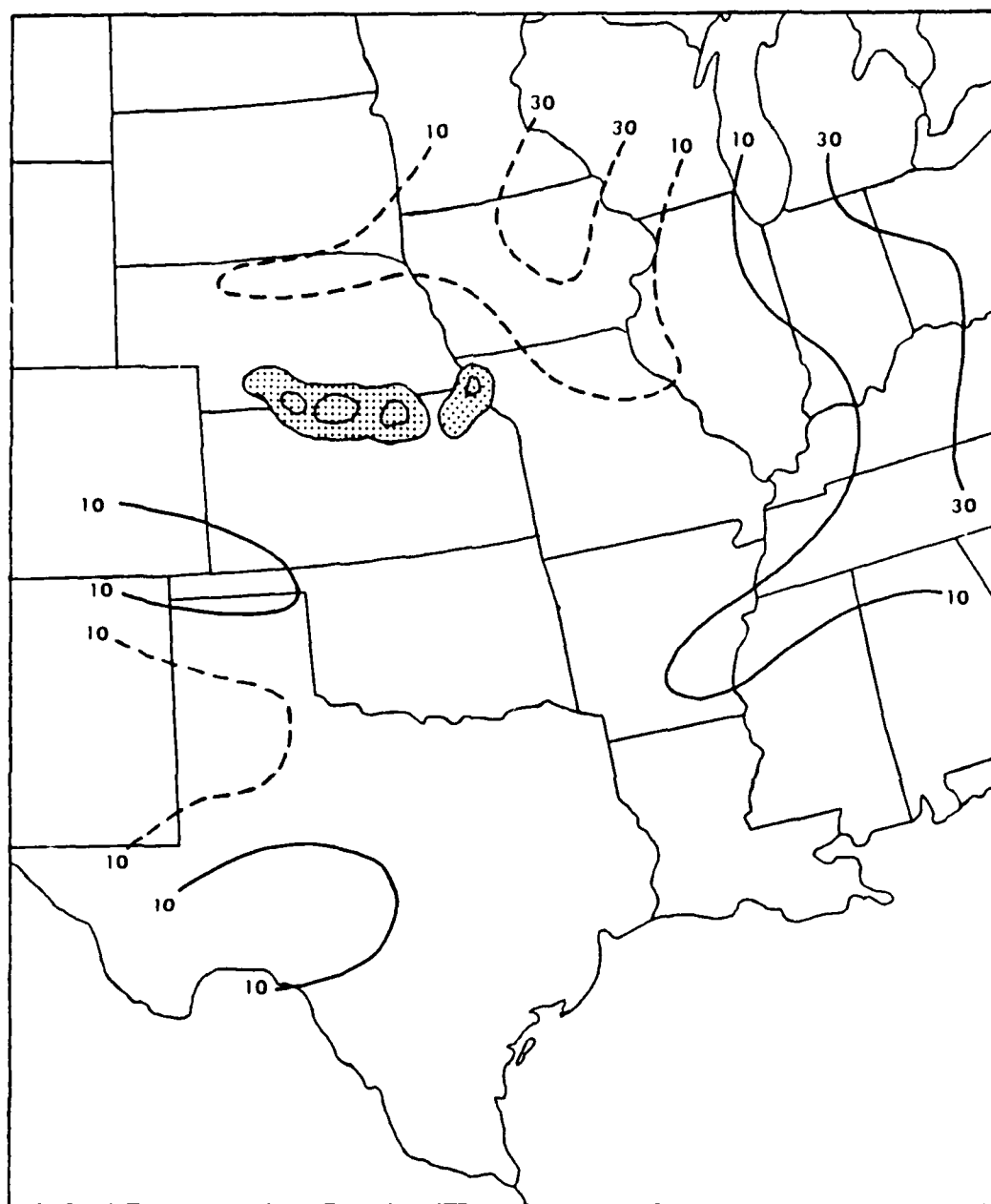
Fig. A-2b. 850 mb water vapor advection ($\times 10^{-2}$ g kg^{-1} h^{-1}) for 0000 GMT 9 August 1978. Solid lines are positive and dashed lines are negative. Stippled region depicts the non-MCC radar echo at 0435 GMT.
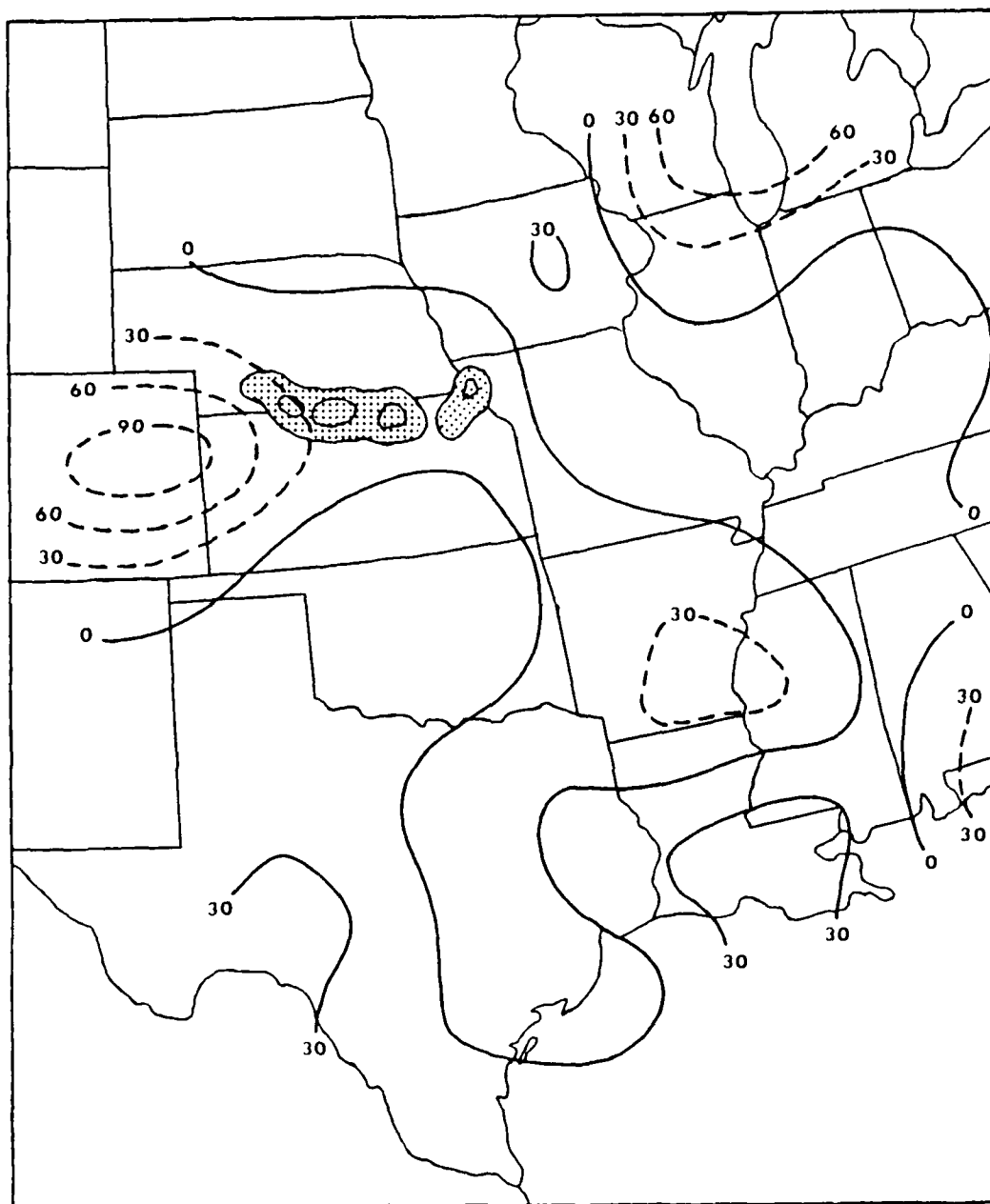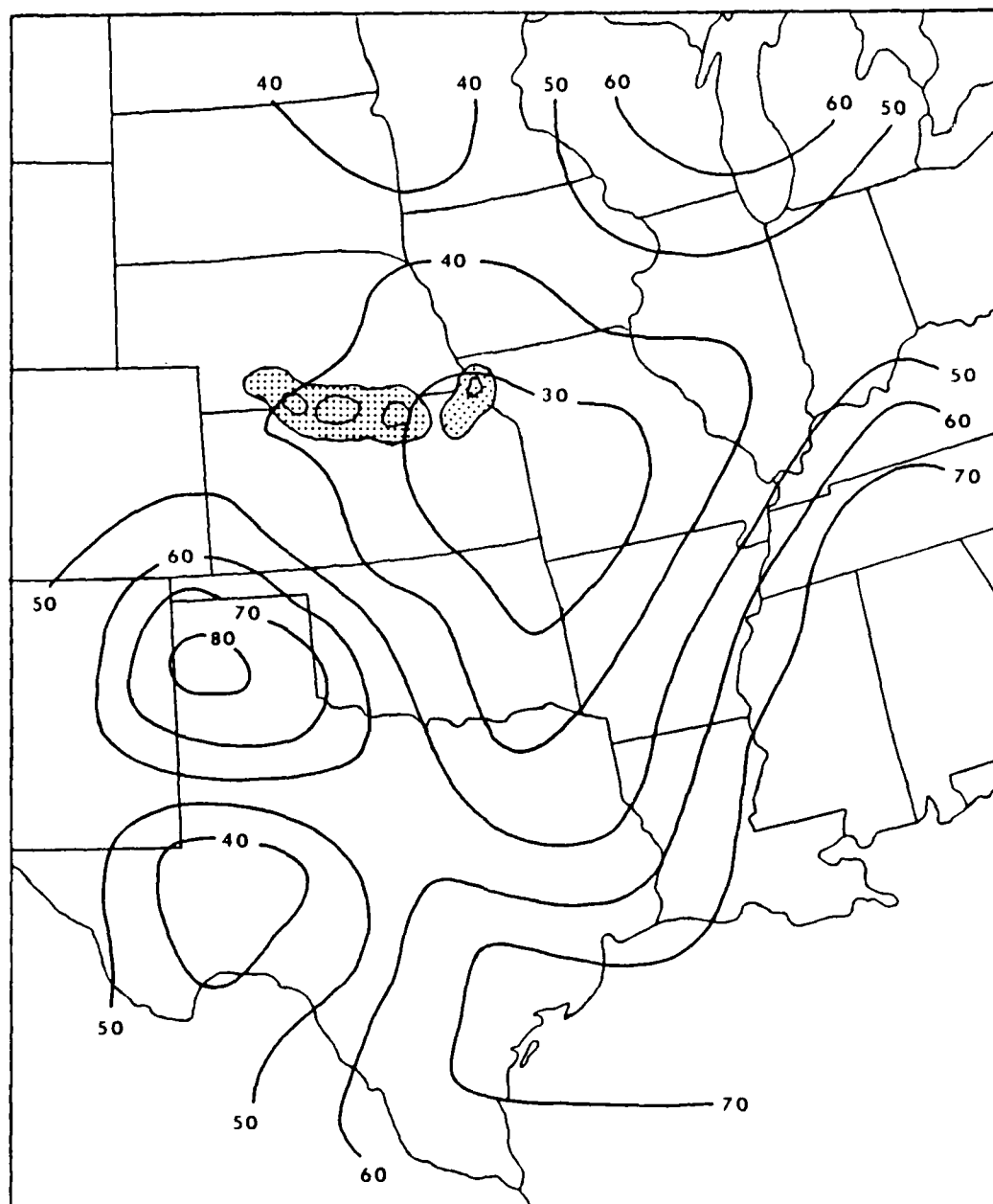
Fig. A-2c. 850 mb flux divergence of water vapor ($\times 10^{-2}$ g kg^{-1} h^{-1}) for 0000 GMT 9 August 1978. Solid lines are positive and dashed lines are negative. Stippled region depicts the non-MCC radar echo at 0435 GMT.

Fig. A-2d. Surface-to-500 mb average relative humidity (%) for
0000 GMT 9 August 1978. Stippled region depicts the non-MCC radar echo
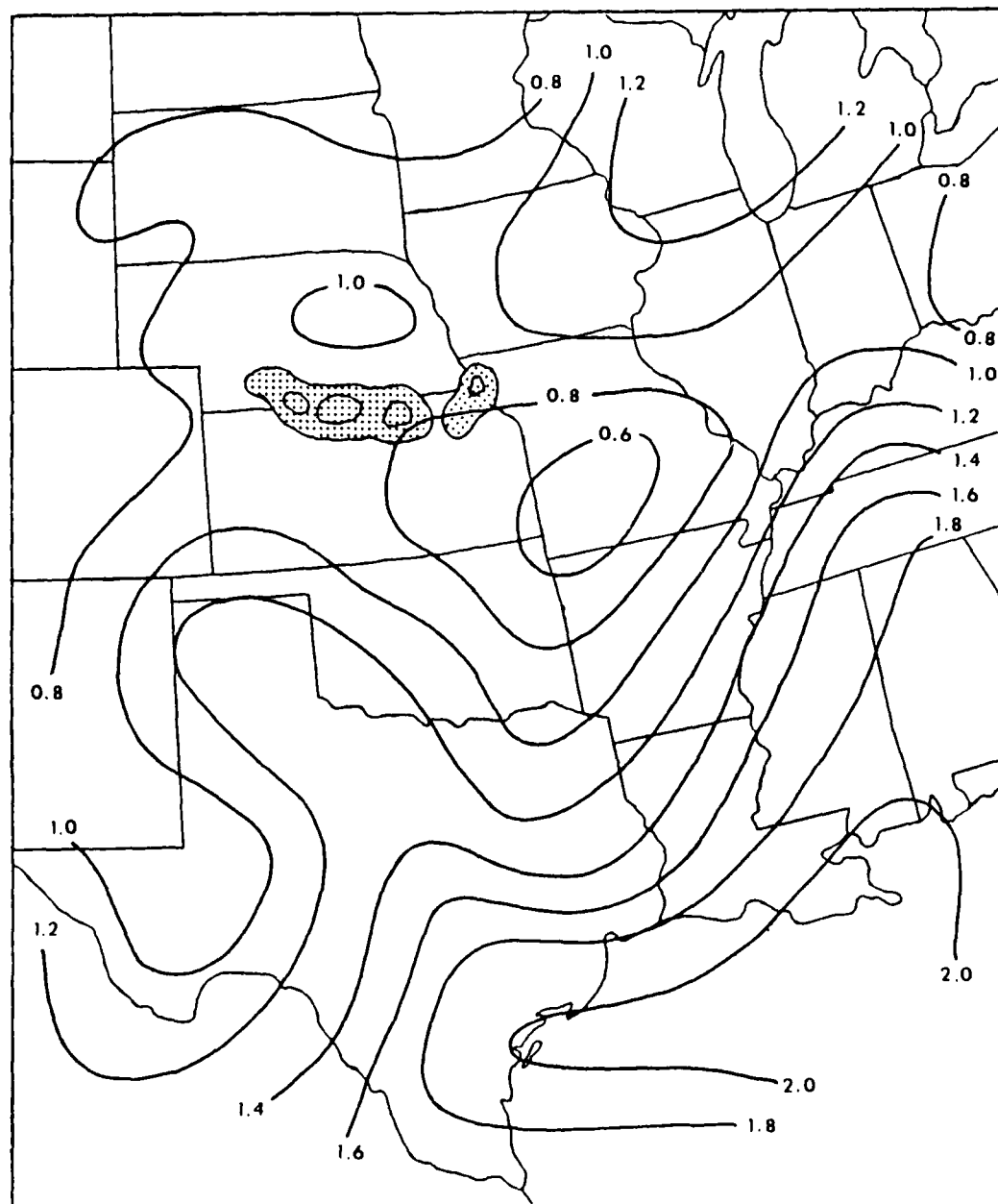at 0435 GMT.

Fig. A-2e. Precipitable water (inches) for 0000 GMT 9 August 1978. Stippled region depicts the non-MCC radar echo at 0435 GMT.
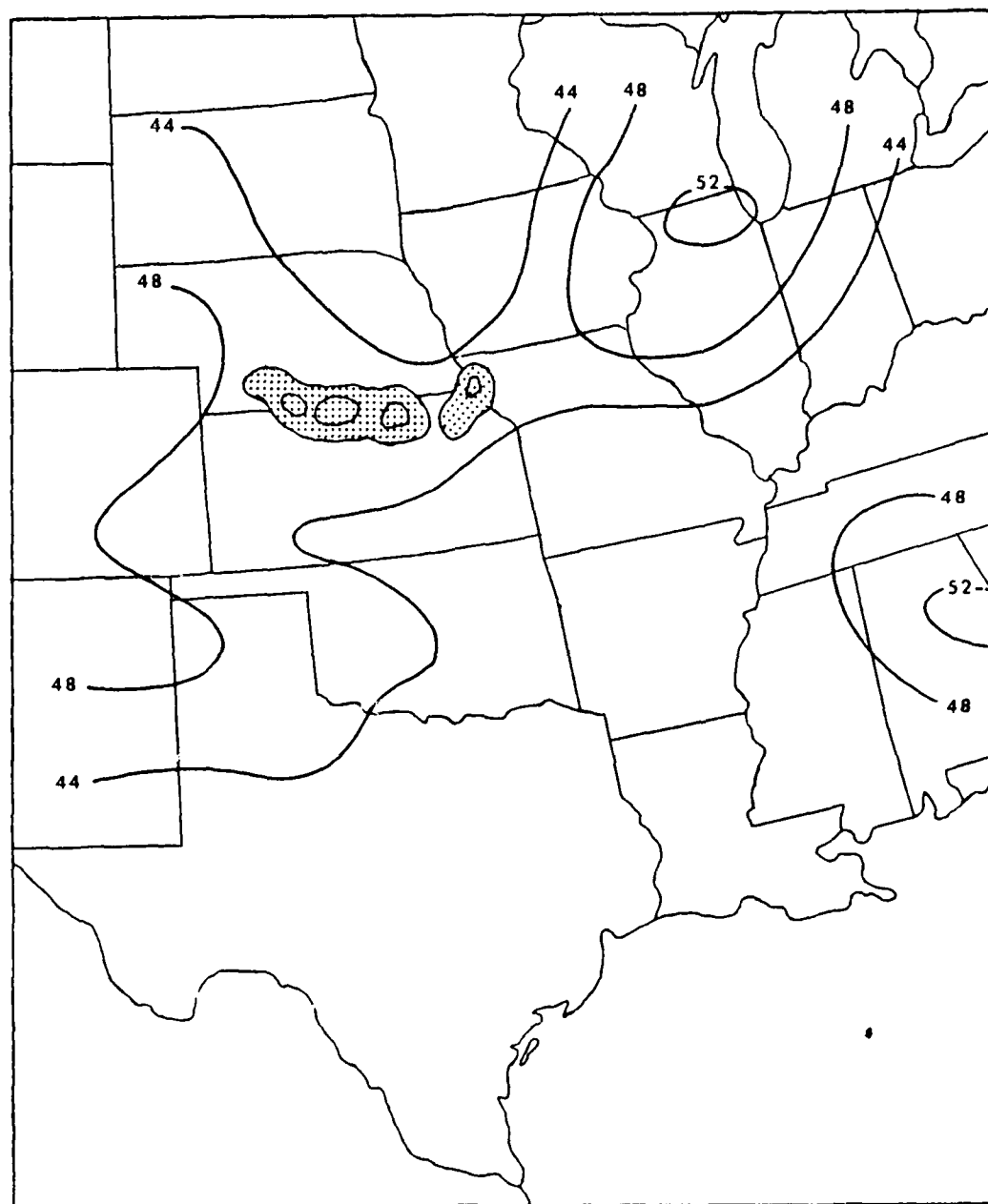
Fig. A-2f. Totals Index for 0000 GMT 9 August 1978. Stippled region depicts the non-MCC radar echo at 0435 GMT.
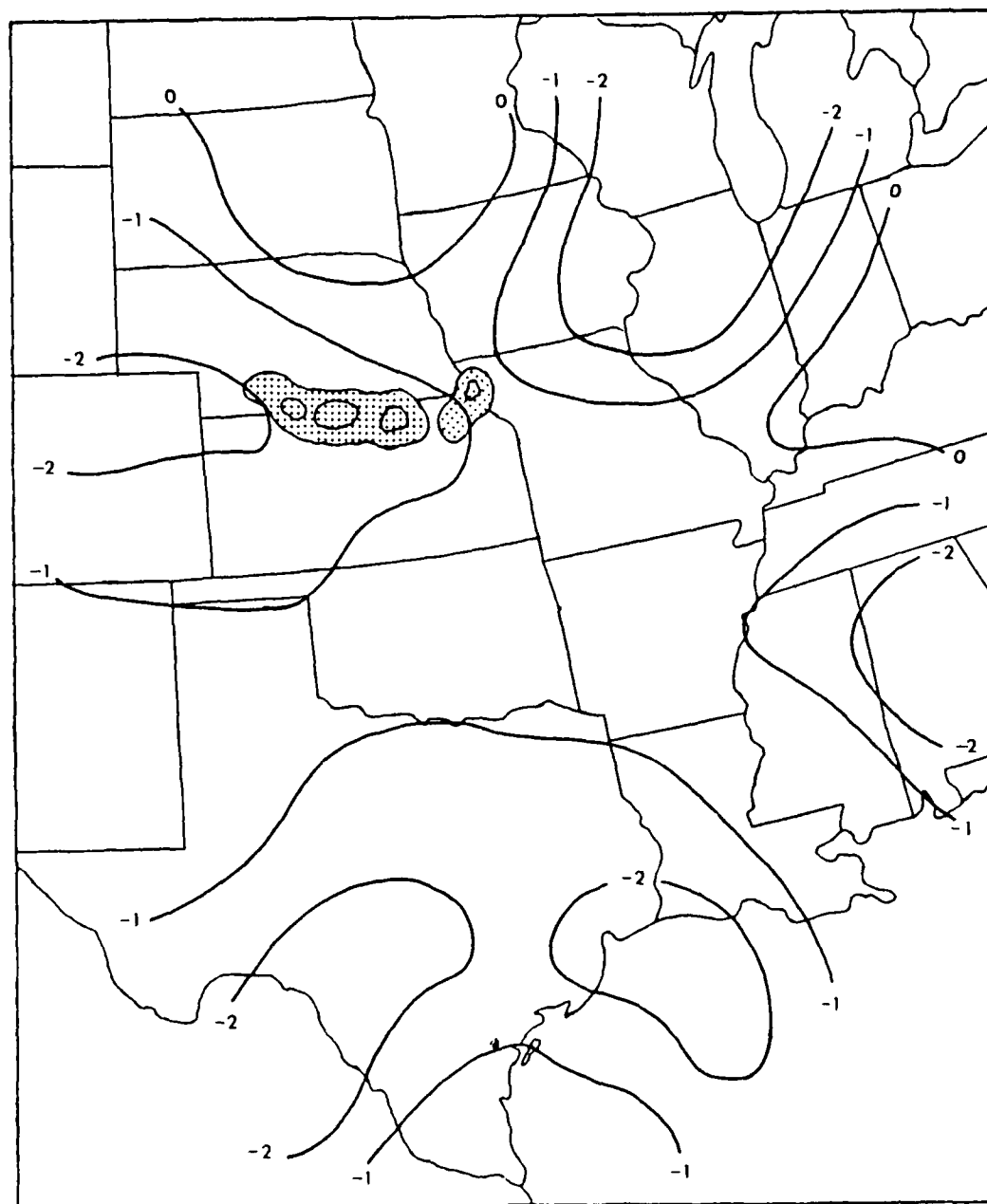
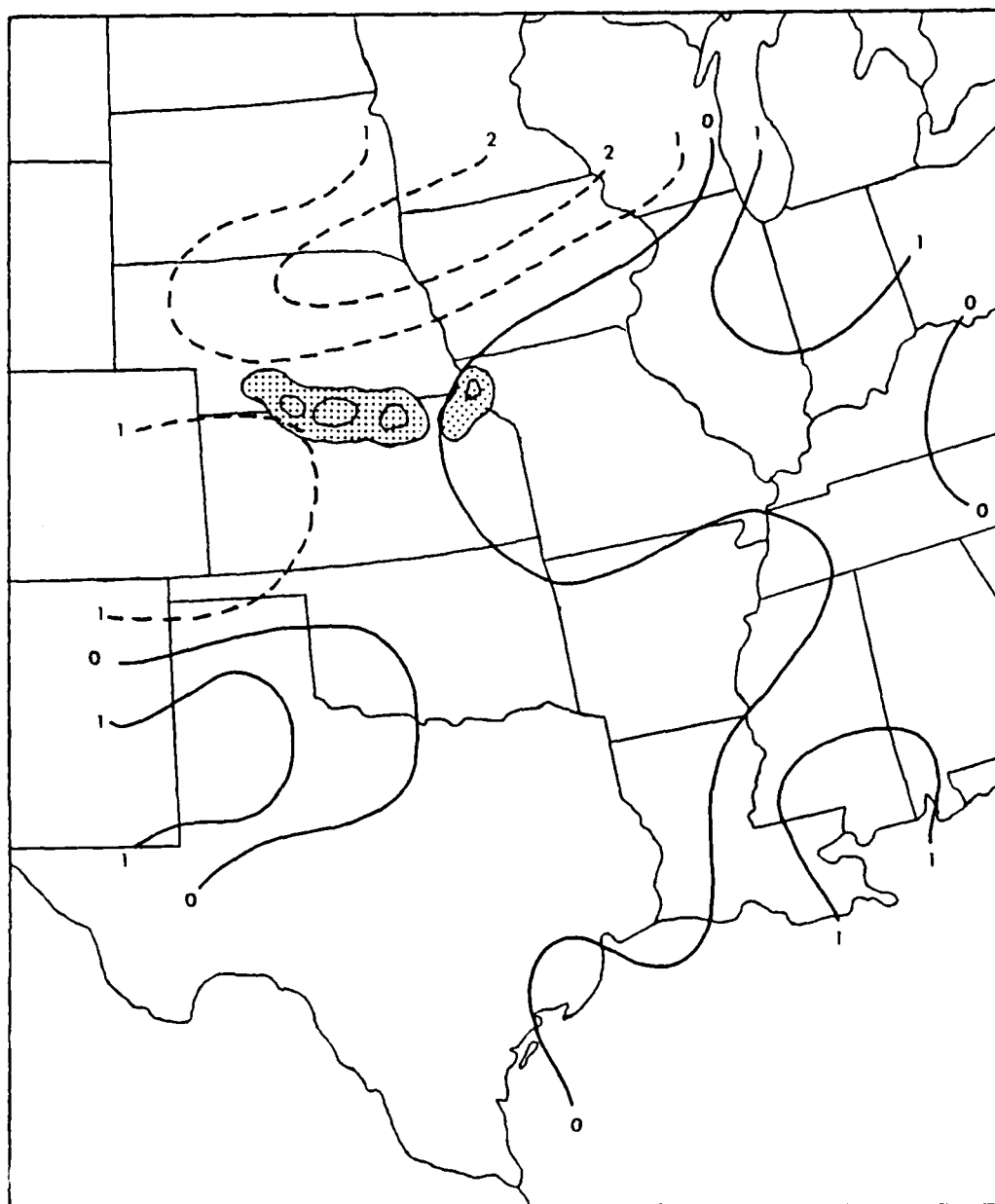Fig. A-2g. Total Energy Index (cal g^{-1}) for 0000 GMT 9 August 1978. Stippled region depicts the non-MCC radar echo at 0435.

Fig. A-2h. 1000-700 mb thickness advection (gpm h^{-1}) by 850 mb wind for 0000 GMT 9 August 1978. Solid lines are positive and dashed lines are negative. Stippled region depicts the non-MCC radar echo at 0435 GMT.

Fig. A-2i. 500-300 mb thickness advection (gpm h⁻¹) by 400 mb wind for 0000 GMT 9 August 1978. Solid lines are positive and dashed lines are negative. Stippled region depicts the non-MCC radar echo at 0435 GMT.
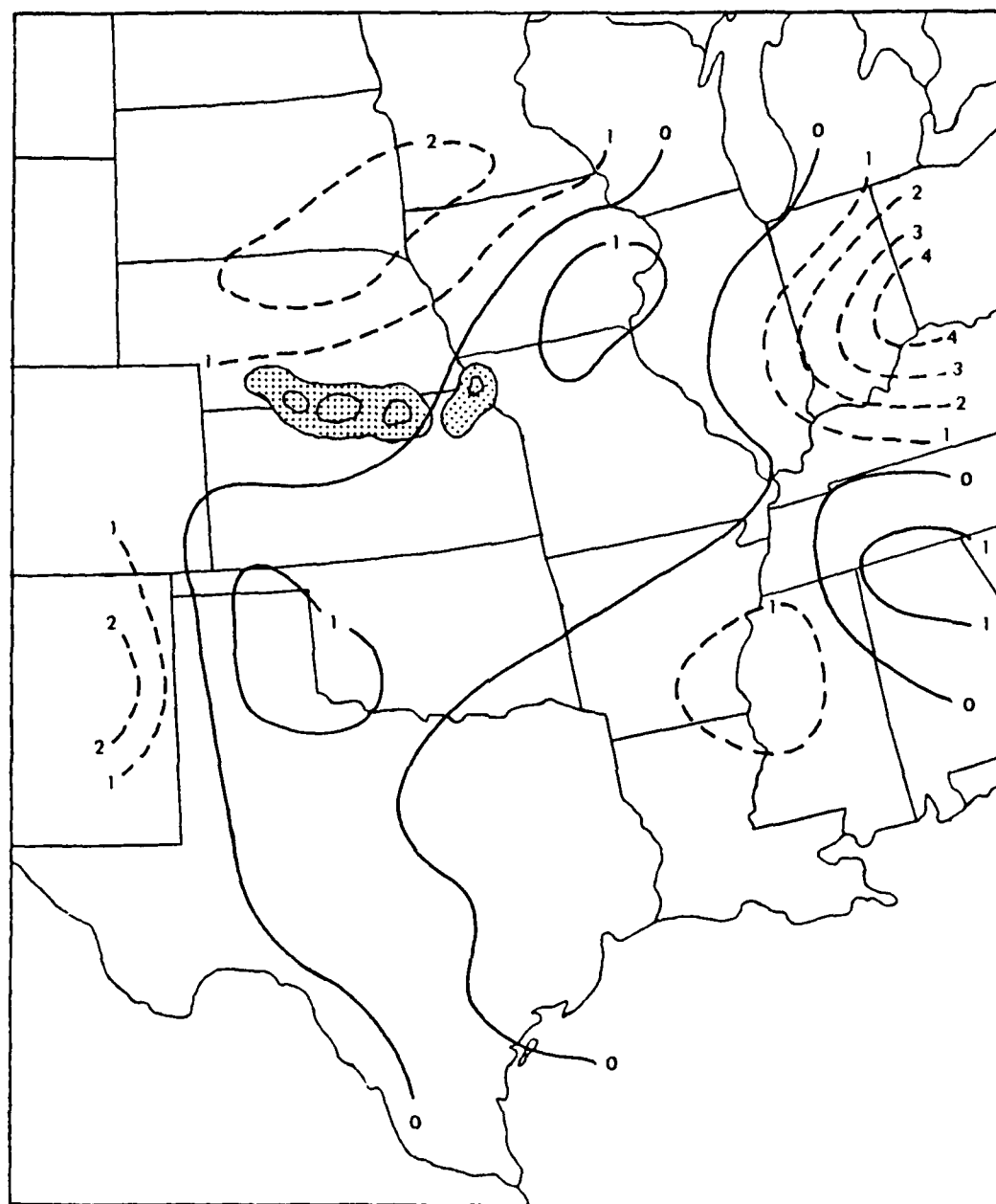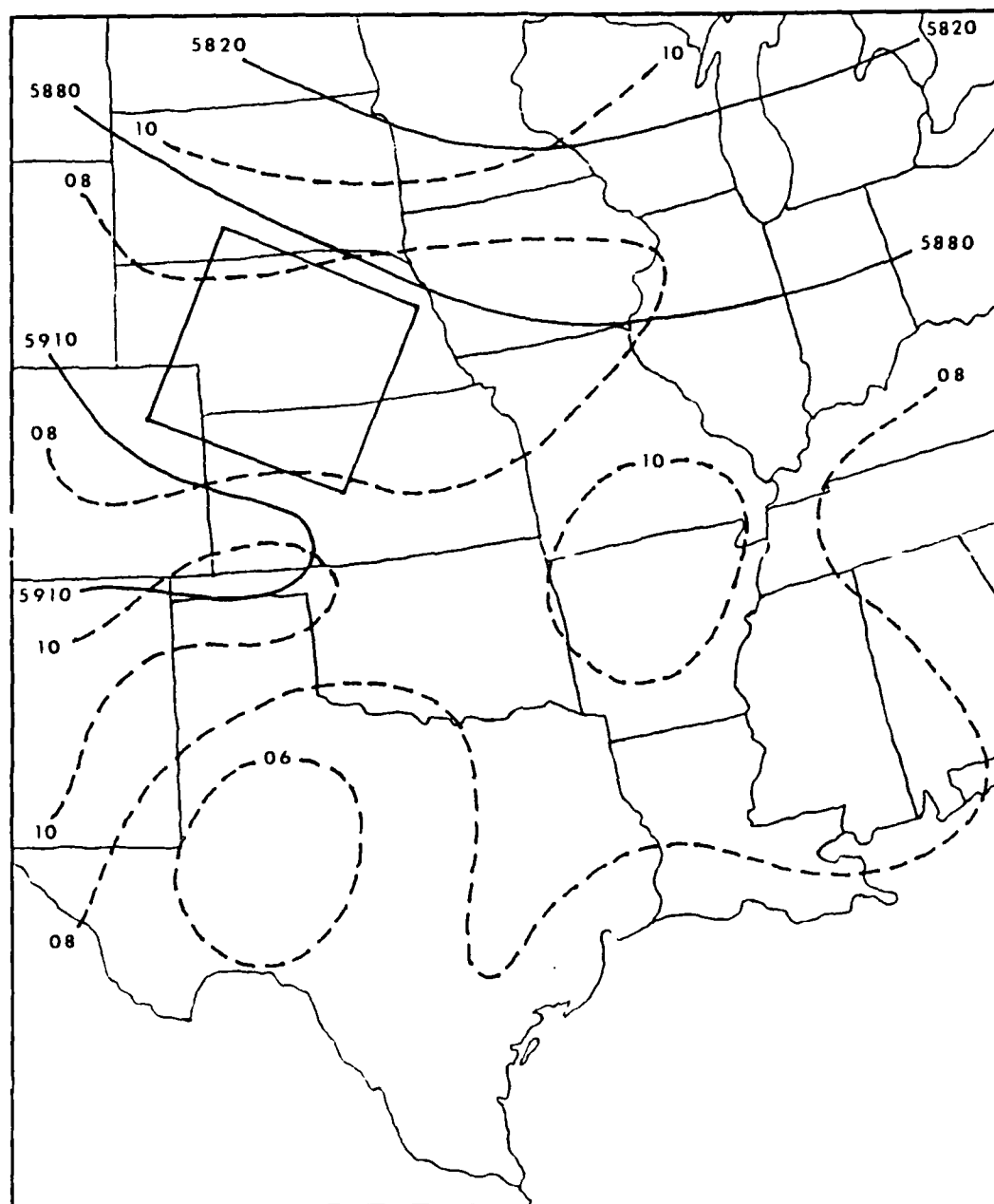
Fig. A-2j. NMC 500 mb Height/Vorticity Analysis Chart for 0000 GMT 9 August 1978. Units are gpm for height (solid lines) and ($x10^{-5}$ s^{-1}) for vorticity (dashed lines). The height/vorticity field within the box was used to estimate the type and intensity of vorticity advection into the non-MCC region.
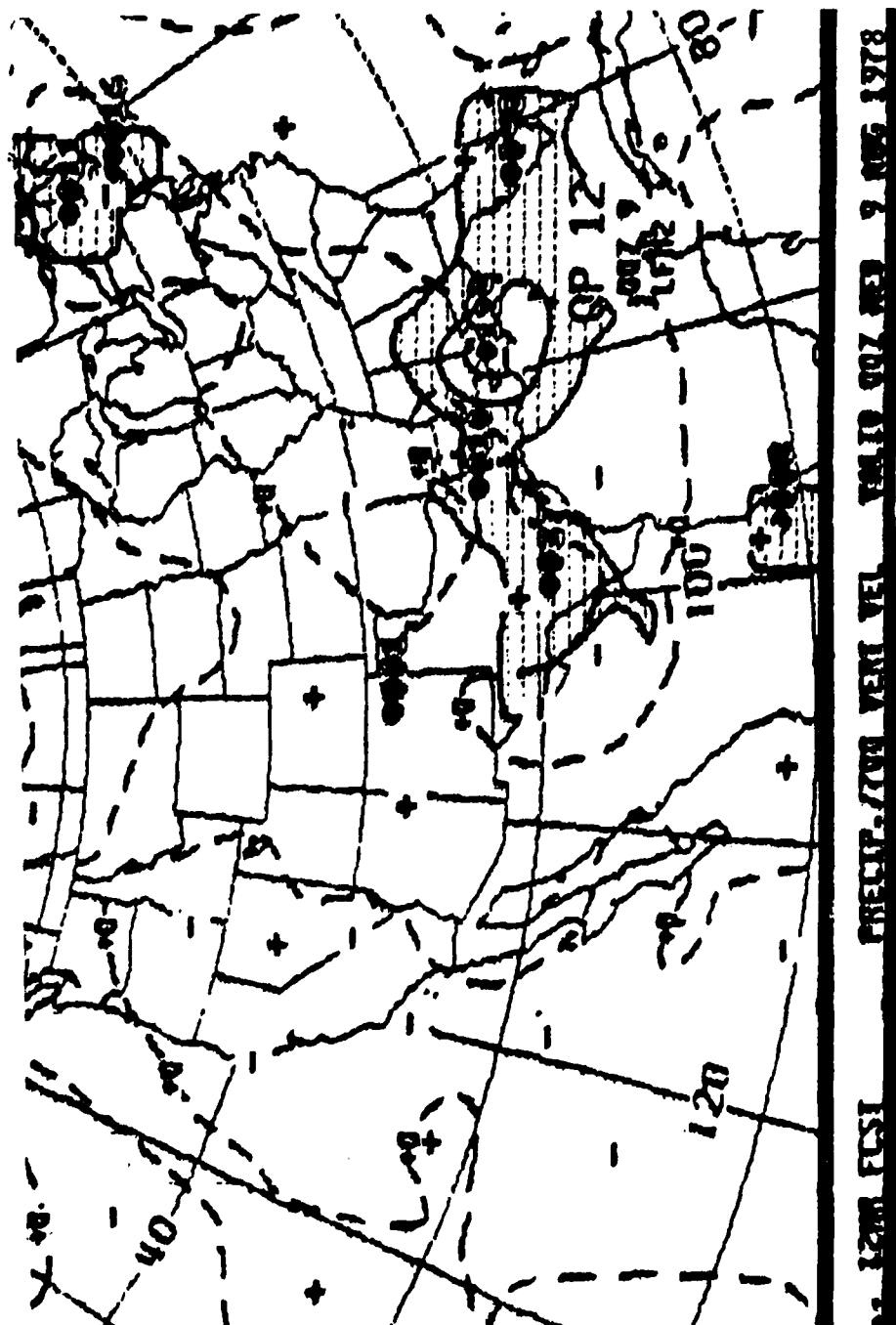
Fig. A-2k. LFM vertical velocity (μb s⁻¹) forecast chart for 0000 GMT 9 August 1978. Iso-lines of vertical velocity are dashed.

APPENDIX B

METHOD USED TO ESTIMATE THE 850 MB ENERGY
RATE OF CHANGE DUE TO THICKNESS AND WATER VAPOR ADVECTION

The static energy (E_s) of a unit mass of air is expressed as

$$E_s = c_p T + Lq + gZ. \tag{B1}$$

It is the sum of specific enthalpy ($c_p T$), latent heat (Lq), and potential energy (gZ). Darkow (1968) approximated this quantity using (B2)

$$E_s \simeq c_p T + L_0 w + gZ \tag{B2}$$

where L_0 is a constant latent heat of condensation and w is the mixing ratio. The energy rate of change is expressed by

$$\frac{dE_s}{dt} \simeq c_p \frac{dT}{dt} + L_0 \frac{dw}{dt} + g \frac{dZ}{dt}. \tag{B3}$$

For this investigation, $\frac{dE_s^*}{dt}$ is defined as the energy rate of change due solely to changes in sensible and latent heat. Thus,

$$\frac{dE_s^*}{dt} \simeq c_p \frac{dT}{dt} + L_0 \frac{dw}{dt}. \tag{B4}$$

Furthermore, if only advective changes are considered, (B4) becomes

$$\left(\frac{\Delta E_s^*}{\Delta t}\right)_{adv} \simeq c_p \left(\frac{\Delta T}{\Delta t}\right)_{adv} + L_0 \left(\frac{\Delta w}{\Delta t}\right)_{adv} . \qquad (B5)$$

Equation (B5) provides a means for combining low-level thickness and water vapor advection into one physically realistic term. This procedure was applied to each MCC and non-MCC case to obtain estimates of the 850 mb energy rate of change due to advection.

Before (B5) could be used, however, thickness advection values had to be converted to advection values of mean virtual temperature $(\bar{T}^*)$ using the relationship

$$\left(\frac{\Delta \bar{T}^*}{\Delta t}\right)_{adv} = \frac{\left[\frac{\Delta_v(\Delta\phi)}{\Delta t}\right]_{adv}}{K \ln \frac{p_1}{p_2}} \qquad (B6)$$

where K is the hypsometric constant. The expression $\Delta_v(\Delta\phi)$ represents the vertical change in thickness between pressure levels p_1 and p_2. Simplified for calculations, (B5) becomes

$$\left(\frac{\Delta E_s^*}{\Delta t}\right)_{adv} = .24 \left(\frac{\Delta \bar{T}^*}{\Delta t}\right)_{adv} + .586 \left(\frac{\Delta w}{\Delta t}\right)_{adv} \qquad (B7)$$

where units for $\left(\frac{\Delta \bar{T}^*}{\Delta t}\right)_{adv}$ and $\left(\frac{\Delta w}{\Delta t}\right)_{adv}$ are ^oC h^{-1} and g kg^{-1} h^{-1}, respectively. L_0 was selected based upon a typical 850 mb temperature

of 20°C. Units for $\left(\frac{\Delta E_s^*}{\Delta t}\right)_{adv}$, the energy rate of change, are

cal g^{-1} h^{-1}.

VITA

Michael Eugene Hoofard was born May 4, 1953 to Louis and Wanda Hoofard in San Antonio, Texas. He graduated from Edison High School in San Antonio in 1971 and began studies at San Antonio College that same year. Michael then transferred to Texas A&M University where he majored in meteorology. He graduated in August of 1975 with a Bachelor of Science in Meteorology. While at Texas A&M, he was inducted into Chi Epsilon Pi, the meteorology honor society. In August of the following year, he entered Officer Training School and on October 29, 1976 was commissioned as a second lieutenant in the United States Air Force. Before returning in 1983 to Texas A&M for graduate work, Michael was assigned as a forecaster and wing weather officer at McConnell AFB, Kansas and as a weather instructor to navigator trainees at Mather AFB, California. He married Judy Van Straten in 1980 and has one son. Currently, Capt Hoofard is assigned to the 11th Weather Squadron at Elmendorf AFB, Alaska as the aerospace sciences officer.

END

10-86

DTIC